J. Space Weather Space Clim. 2023, **13**, 17

https://doi.org/10.1051/swsc/2023013

JSWSC

Available online at:
www.swsc-journal.org

RESEARCH ARTICLE OPEN ACCESS

The Mansurov effect: Seasonal and solar wind sector structure dependence

Jone Øvretvedt Edvartsen, Ville Maliniemi, Hilde Nesse, and Spencer Hatch

Birkeland Center for Space Science, Department of Physics and Technology, University of Bergen, 5007 Bergen, Norway

Received 10 July 2022 / Accepted 5 May 2023

Abstract – We investigate the connection between the interplanetary magnetic field (IMF) B_y-component and polar surface pressure, also known as the Mansurov effect. The aim of the investigation is to unravel potential dependencies on specific seasons and/or solar wind sector structures, and it serves as a sequel to Edvartsen et al. (2022) [*J Space Weather Space Clim* **12**: 11]. The mechanism for the effect includes the ability of the IMF to modulate the global electric circuit (GEC), which is theorized to impact and modulate cloud generation processes. By usage of daily ERA5 reanalysis data for geopotential height since 1968, we find no significant response confirming the current Mansurov hypothesis. However, we do find statistically significant correlations on decadal timescales in the time period March–May (MAM) in the northern hemisphere, but with an unusual timing. Similar phased anomalies are also found in the southern hemisphere for MAM, but not at a significant level. In an attempt to explain the unusual timing, heliospheric current sheet crossing events, which are highly correlated with the B_y-index, are used. These events result in higher statistical significance in the NH for the MAM period, but cannot fully explain the timing of the response. In general, these statistically significant correlations differ from previously reported evidence on the Mansurov effect, and suggest a revision of the Mansurov hypothesis. Our results also highlight a general feature of time-lagged cross-correlation with autocorrelated variables, where the correlation value itself is shown to be a fragile indicator of the robustness of a signal. For future studies, we suggest that the *p*-values obtained by modern statistical methods are considered, and not the correlation values alone.

Keywords: Solar-climate link / Significance testing / Monte-Carlo / False-detection-rate / Periodic forcing

1 Introduction

The hypothesis on the Mansurov effect, which assumes a relation between daily polar surface pressure and the B_y-component of the interplanetary magnetic field (IMF), was first proposed by Mansurov et al. (1974). Multiple studies have found a correlation supporting this hypothesis in more recent times (Burns et al., 2008; Lam et al., 2013, Lam & Tinsley, 2016; Zhou et al., 2018; Tinsley et al., 2021; 2018). However, Edvartsen et al. (2022) found the previous correlations to be below the 95% statistical significance limit. Moreover, the 27-day cyclic response, which has previously been used as evidence for the effect (Burns et al., 2008; Lam et al., 2018; Tinsley et al., 2021), was shown to occur as a statistical artifact due to the periodic B_y-forcing and high autocorrelation in the surface pressure. This work aims at investigating the open ends not addressed by Edvartsen et al. (2022), mainly, the potential for a seasonal and/or solar structure dependency for the link between B_y-forcing and polar surface pressure response.

The Mansurov hypothesis assumes a positive (negative) correlation between B_y and surface pressure anomalies in the Southern (Northern) Hemisphere. The effect is thought to arise in connection with the Global Electric Circuit (GEC). The GEC links the electric fields and currents flowing in the lower atmosphere, ionosphere, and magnetosphere to form a global spherical conductor (Siingh et al., 2007). Global thunderstorms act as batteries charging the GEC by generating upward-driven currents J_z. In addition to electrified clouds, this maintains an average potential difference (V_i) between the ionosphere and the Earth's surface at about 250 kV (Tinsley, 2000; Williams, 2005). In fair weather regions, a return current (J_z) flows in the direction ionosphere–surface, thereby completing the GEC. When the velocity of the solar wind ($\mathbf{V}$) flows radially outwards from the sun with its frozen in the magnetic field ($\mathbf{B}$), relative to the Earth, this gives rise to a $\mathbf{V} \times \mathbf{B}$ motional electric field as seen by an observer stationed at Earth. Through the conducting magnetic field lines, the potential of the electric

*Corresponding author: jone.edvartsen@uib.no

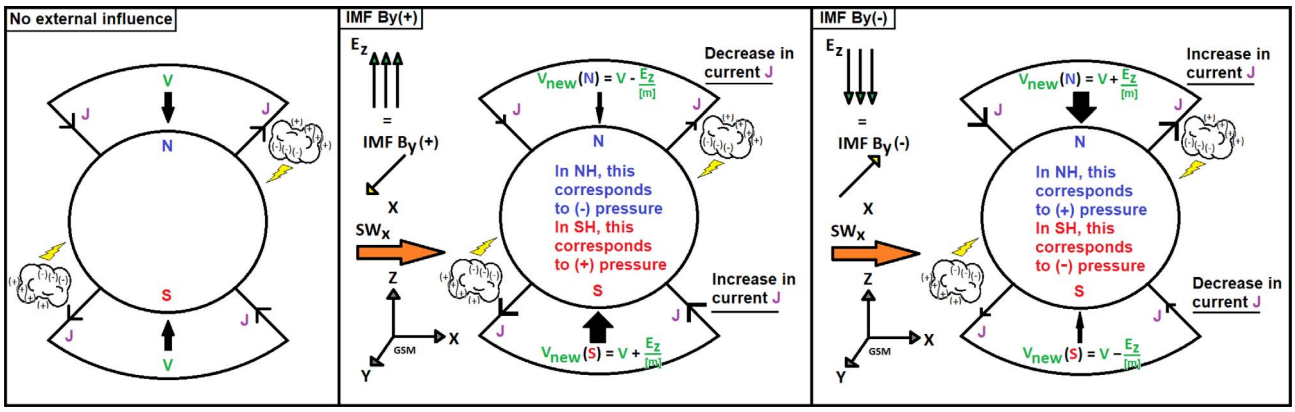

Fig. 1. IMF B_y(+) leads to a decrease in V and J in the NH and an increase in V and J in the SH. IMF B_y(–) leads to an increase in V and J in the NH, and a decrease in V and J in the SH. Relating this to the Mansurov-associated pressure changes means that an increase in the ionospheric potential and fair weather current leads to an increase in pressure.

field is superimposed on the global ionospheric potential V_i (Tinsley, 2008). In Geocentric Solar Magnetospheric (GSM) coordinates a magnetic field in the y-direction (B_y) gives rise to a potential difference between the northern polar cap ionosphere and the southern polar cap ionosphere of typically a few tens of kV (Tinsley & Heelis, 1993). As the ionospheric potential V_i changes, so does the fair weather current J_z. Figure 1 shows an illustration of the components involved in the mechanism, mainly the perturbation of the ionospheric potential and the effect on J_z.

Tinsley (2008) also discusses other sources able to modulate J_z and then links to atmospheric changes. Studies have found a relation between Galactic Cosmic Rays (GCR) and cloud cover over decadal timescales (Tinsley, 2008; Veretenenko & Ogurtsov, 2012; Veretenenko et al., 2018). Correlations have also been found between internally driven modulations of J_z (thunderstorm generator) and atmospheric pressure changes, which are together known as the Burns effect (Burns et al., 2007, 2008; Zhou et al., 2018). It is suggested that all these mechanisms, through the modulation of the ionospheric fair weather current J_z, affect microphysical processes in clouds (Tinsley, 2022). As the currents flow through high gradients of conductivity across cloud boundaries they add to the separation of positive and negative ions. These ions can attach to aerosols and droplets, where they influence microphysical processes due to the Coulomb interaction (Tinsley & Deen, 1991; Tinsley, 2000, 2008). The influence on the microphysics of clouds should occur nearly instantaneously. However, this effect is relatively small, and it is predicted that the microscale changes take days before materializing as macro-physical changes in cloud radiative properties. Furthermore, after manifesting, these radiative changes might lead to pressure responses observed at the surface level (Frederick et al., 2019; Tinsley et al., 2021).

Both the atmosphere and the solar wind are highly variable in nature, potentially leading to different surface responses during different conditions. Tinsley et al. (2021) show an intensified relation between B_y and the surface pressure anomaly during local northern winter. However, no significance estimation is assessed. Zhou et al. (2018) found that during four years from 1998 to 2001, the correlation between the vertical electrical field and surface pressure is larger during local winter in both hemispheres. For the variability in the solar wind, Tinsley et al. (2021) found that cloud irradiance over Alert, Canada was larger when the solar wind structure was two-sector (IMF B_y oscillating at a 27-day period), compared to four-sector (IMF B_y oscillating at a 13.5-day period). It is also highlighted that the most cited period in favor of the Mansurov effect, 1999–2002, is dominated by two-sector structures. In our work, we will focus exclusively on the Mansurov effect. We seek to determine whether there is statistically significant evidence in favor of its existence, and therefore confine attention in this study to the correlation between IMF B_y and surface pressure. We do not attempt to comment on the viability of any particular mechanism. In contrast to our previous work (Edvartsen et al., 2022), where we questioned the statistical significance of the effect on the basis of analysis of continuous decadal timescales, we now address the potential seasonal and solar wind sector structure dependence.

2 Data and method

2.1 Solar wind (B_y) data

We use daily averaged IMF B_y (Geocentric Solar Magnetospheric, GSM, coordinates) values obtained from the National Space Science Data Center (NSSDC) OMNIWeb database (http://omniweb.gsfc.nasa.gov) for the interval 1968–2020. In this coordinate system, X points along the Sun–Earth line, Z points along Earth's magnetic dipole axis, with Y perpendicular to both X and Z.

2.2 Pressure/geopotential height data

For the atmospheric data, we use the European Center for Medium-Range Weather Forecast Re-Analysis (ERA5) (https:// cds.climate.copernicus.eu). These data are constructed by interpolating observations with numerical simulations and models, effectively constructing a high-resolution atmospheric database. It is noted that reanalysis data does not have the accuracy as pure observational data at every grid point. Nevertheless, it still allows for a physically justified approximation in the grids where observations are not accessible. Multiple studies have used reanalysis data in the examination of the Mansurov effect (Lam et al., 2013, 2018; Zhou et al., 2018; Freeman & Lam,

2019; Edvartsen et al., 2022), justifying its usage for the purpose of this study.

We focus on the geopotential height of the 700 hPa level in both hemispheres. In the SH this represents the surface, while in the NH this represents a few kilometers above surface level. The geomagnetic perturbations of IMF B_y in the ionosphere are centered around the geomagnetic pole. Therefore, the geopotential height will be averaged to one value for each hemisphere from 70° poleward in geomagnetic coordinates (mlat). The full data period covers the time period 1968–2020. To account for seasonal variability, a perturbation value is obtained for each hemisphere ($Z_{g(\mathrm{NH})}$ and $Z_{g(\mathrm{SH})}$). These are obtained by subtracting a running mean of ±15 days from the daily value of the geopotential height data series.

2.3 Modern statistical methods

Analogous to Edvartsen et al. (2022), we use Monte Carlo (MC) simulation together with the false discovery rate (FDR) method to estimate the statistical significance. The MC approach handles the uncertainty introduced by temporal autocorrelation. The FDR method tests multiple null hypotheses simultaneously, namely the expected increase in falsely rejected null hypotheses at the 5% level as the number of hypotheses itself increases. The following sections provide details on how the MC and FDR methods are implemented in this study.

2.3.1 Monte Carlo approach

The main goal of the MC approach is to construct a repeated analysis with similar statistical conditions as found in the original data series, however, with an introduced element of randomness for each iteration. The process results in a distribution of simulated results where the null hypothesis is assumed to hold. As such, original findings can be compared to the fraction of as extreme or more extreme simulated results to obtain the p-value, which then becomes the likelihood of obtaining a similar result by chance.

The main investigative tool used in our study is the time-lagged cross-correlation method (Pearson linear correlation coefficient). It correlates two different data series (forcing and response), with an introduced shift with respect to each other in the temporal direction. The method can therefore identify directionality (forcing → response) between the data series, as well as the associated time lag. The MC significance test can be implemented by replacing the response data series with surrogate data while keeping the forcing data identical. The surrogate data have to be statistically equivalent in terms of statistical features (e.g. autocorrelation, standard deviation, mean, etc.). Lancaster et al. (2018) provide a technical overview of different ways to create simulated data. We use the Fourier transform (FT) method, which is computationally cheap and easy to implement, and proceeds as follows: First the FT (ft_x) of the original response data series, the geopotential height, is calculated. Then, a random phase vector (ϕ_r) is generated. As the FT is symmetrical, the new phase randomized vector (ft_r) can be obtained by multiplying the first half of ft_x by $\mathbf{exp}(i\phi_r)$ (this corresponds to the positive frequencies). The second half of ft_r is then computed by horizontally flipping the complex conjugate of the first half. Finally, the inverse Fourier transform of ft_r gives the FT surrogate data. This method was initially introduced to test for non-linearity in data. It has, however, been shown by e.g. Theiler & Prichard (1996) that the FT-based method provides a good surrogate technique alternative when the statistics of interest are not pivotal, meaning that the distribution of targeted values (correlation value in our case) under the null hypothesis is unknown.

Figure 2 displays the results of the FT-method performed for the geopotential height data series at the 700 hPa level averaged over 70°–90° S for the period 1968–2020. The top left panel shows the raw geopotential height data plotted against time, while the bottom left panel shows the surrogate data after the FT-procedure. In the middle panels, the autocorrelation function for the raw (top) and surrogate data (bottom) are shown, while the right panel shows the power spectrum of the raw (blue) and surrogate data (red). As expected, the FT-method produces a physically unrelated surrogate data series, however, it retains the necessary statistical conditions like autocorrelation (which implies the same number of independent data points), power spectrum, and other features such as standard deviation, variance, and mean (not shown).

This procedure requires continuous data. However, investigating the seasonal dependence of the response in December, January, and February (DJF), requires that these portions of the full continuous data period be extracted. To produce the surrogate data representing the geopotential height for every DJF, we perform the FT-procedure on every individual DJF period before finally stitching the surrogate data together to form a single data series (|DJF|DJF|DJF|...). This is computationally expensive, but necessary to avoid introducing artificial frequencies not found in the original data.

2.3.2 False-discovery rate

The FDR is an appropriate tool when testing multiple null hypotheses simultaneously. When testing a null hypothesis in isolation, the p-value obtained by our MC approach defines the probability of obtaining a result at least as extreme as the observed result, under the assumption that the null hypothesis holds. For example, the common $p = 0.05$ threshold implies that there is a 5% probability of obtaining a given result under the assumption that the null hypothesis is correct. When N null hypotheses are tested (e.g., map plot with multiple grids or time-lagged cross-correlation with multiple lead-lags), the probability of falsely rejecting at least one null hypothesis increases as pN increases. The FDR method, developed by Benjamini & Hochberg (1995) and later applied to atmospheric sciences by Wilks (2016), aims to account for the increase in the expected rate of falsely rejected null hypotheses as N increases.

In its simplest form, the FDR method assumes statistically independent null hypotheses and an identical distribution of observations (i.e., the data characteristics, such as the mean, median, and standard deviation, are the same for every group or sample being compared). When dealing with atmospheric data such as geopotential height, high autocorrelation exists, both temporally (Fig. 2 middle panels) and spatially. In a time-lagged cross correlation plot or map plot with multiple grids, each data point will therefore not be statistically independent. To address this issue, Wilks (2016) improved on the approach developed by Benjamini & Hochberg (1995), by introducing a factor that accounts for the autocorrelation in the data. The full process involves the computation of p-values

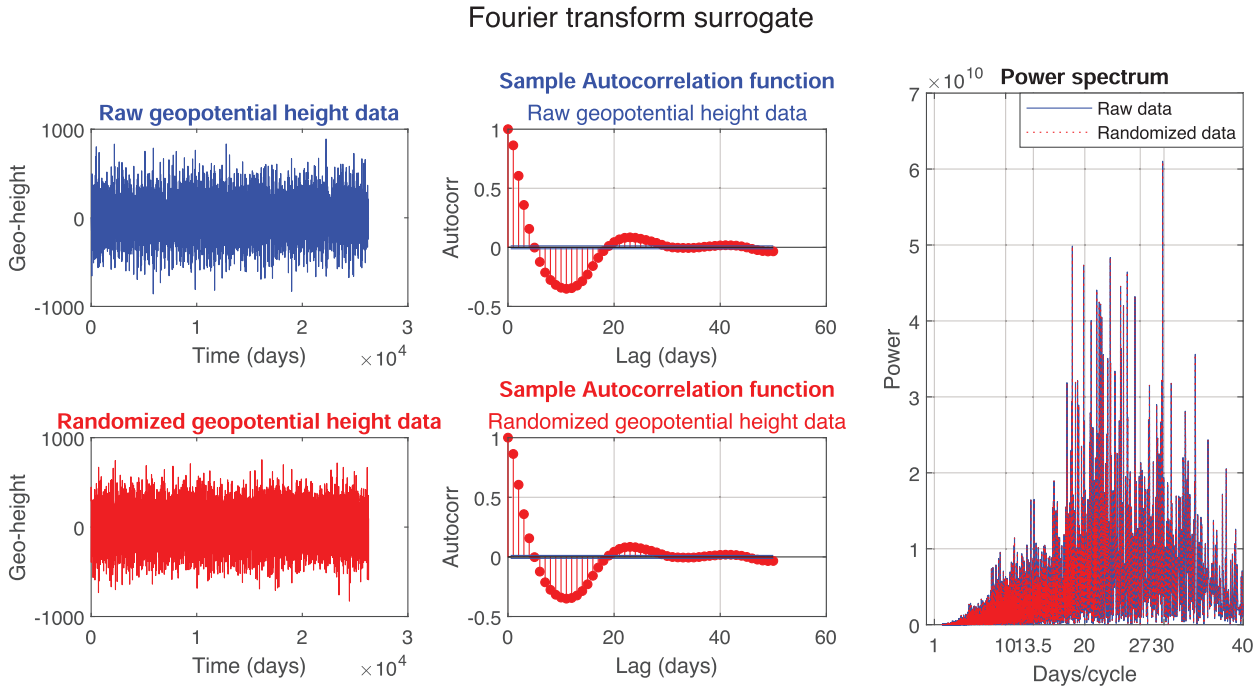

Fig. 2. *Left panels*: Raw geopotential height data series at the 700 hPa level averaged over 70°–90° S for the period 1968–2020 (top panel), and the FT surrogate (bottom panel). *Middle panels*: Autocorrelation function of the raw (top) and FT surrogate (bottom) geopotential height data. *Right panel*: Power spectrum of the raw data (blue) and the FT surrogate (red). As can be seen, there is an identical match for the autocorrelation and the power spectrum.

for each data point (MC-approach), before sorting them in ascending order. The sorting forms the set $i = 1, \ldots, N$ where N represents the total number of individual null hypotheses to be tested. A new global p-value, p_{FDR}, is then calculated by iterating through the individual p-values starting at the lowest, and looking for the last p-value fulfilling the equation:

$$p_{\mathrm{FDR}} = \max[p(i) : p(i) \leq (i/N)\alpha_{\mathrm{FDR}}], \quad i = 1, \ldots, N. \quad (1)$$

In case of independent individual null hypotheses, $\alpha_{\mathrm{FDR}} = 0.05$ ensures that the global p-value (p_{FDR}) is correctly interpreted at the 95% confidence level. The statistical significance of individual tests is determined by comparing their original p-values against the threshold value p_{FDR}. Only those tests with p-values equal to or lower than p_{FDR} are considered statistically significant. However, as discussed, individual data points in a time-lagged cross-correlation plot or map grid plot are not independent. Wilks (2016) demonstrates that for autocorrelation commonly found in atmospheric data, an e-folding distance of $1.54{\cdot}10^3$ km, setting $\alpha_{\mathrm{FDR}} = 0.1$ corrects for dependence between data points and ensures that the p_{FDR} threshold is exceeded in only 5% of the cases globally.

We can calculate which α_{FDR} value is appropriate for our specific data. This analysis will also give insight into how the FDR approach (Wilks, 2016) works at a global scale. The left panel of Figure 3 shows the distribution of correlation values constructed based on an MC-simulation with 20,000 iterations. The distribution of correlation values is made by cross-correlating the real IMF B_y for the period 1968–2020 with surrogate data made from the geopotential height (700 hPa level averaged over 70°–90° S for the same time period) with the FT method for lead-lags −20 to 20. Then, we perform another 20,000 iterations of the same setup. In the right panel, the results from the new iterations are compared against the distribution to the left to calculate the p-value at each specific lead lag for each individual iteration. Simultaneously, the FDR approach is applied to the p-values for each iteration, where five different values for α_{FDR} are tested. When $\alpha_{\mathrm{FDR}} = 0.09$, only 5% of the iterations obtains p-values passing the global FDR threshold. In other words, for our specific data, when α_{FDR} is set to 0.09, 5% of global responses will pass the FDR test when the null hypothesis is assumed correct. Therefore, $\alpha_{\mathrm{FDR}} = 0.09$ will be used in analyses conducted in this study. The requirement of identical distribution of the observations will also be valid in our case. The left panel of Figure 3 shows that all lead-lags have near identical distribution of correlation values after the MC simulation. They have also similar statistical features, such as standard deviation, mean, and median, in the geopotential height data series for two consecutive days. They only diverge slightly with increasing intervals between the days being compared (e.g., winter months tend to exhibit greater variance than summer months). However, since the lead-lag plots in our study are limited to a maximum of 41 days, the distribution of observations can be considered approximately identical.

2.3.3 False-discovery rate in combination with Monte Carlo approach

The FDR method (Eq. (1)), requires a minimum p-value to reject the global null test. For example, if 50 data points are analyzed with $\alpha_{\mathrm{FDR}} = 0.05$, the first sorted p-value must be lower than or equal to $(1/50){\cdot}0.05 = 0.001$. Assuming the null

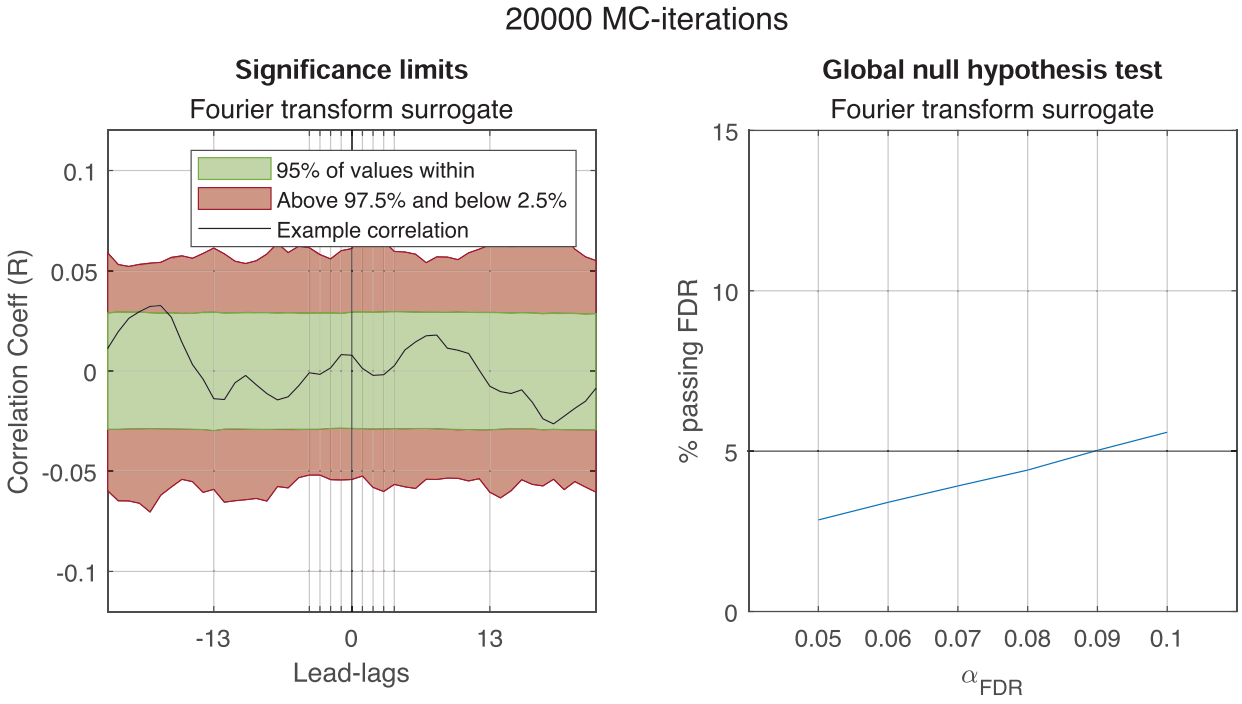

Fig. 3. *Left panel*: Surrogate data (FT-method) made from the raw geopotential height data series at the 700 hPa level averaged over 70°–90° S cross-correlated with the real IMF B_y index over the time period 1968–2020 for 20,000 iterations. The result of these iterations makes up a distribution of correlation values for every lead lag. The red area illustrates where only 5% of correlation values land, while the green shaded area illustrates where the remaining 95% of correlation values land. The black line is added as an example and shows a typical iteration when the surrogate data and B_y are cross-correlated. *Right panel*: After constructing the distribution of correlation values shown in the left panel, the surrogate data and B_y are again cross-correlated 20,000 times. Then, all data points at specific lead lags are measured against the distribution (in left panel) at the specific lead lag to obtain the *p*-values. To accurately estimate the appropriate α_{FDR} in a way that takes into account the autocorrelation present in our data, all *p*-values generated from each iteration of the simulation are processed through the FDR method, where 5 different values for α_{FDR} are tested. By doing so, we can obtain the specific α_{FDR} value which ensures that any signal determined to be statistically significant occurs globally in only 5% of cases when the null hypothesis is assumed to be true for our data. As can be seen, when α_{FDR} is set to 0.09, only 5% of the 20,000 iterations produce a response that passes the global FDR limit.

hypothesis holds, the distribution of *p*-values will be uniform. Therefore, obtaining a *p*-value of 0.001 is a 1/1000 event. If one has exactly 1000 tries, the probability of obtaining the 1/1000 event can be calculated as follows:

Probability that one MC iteration will not be the 0.001 event

$$= 1 - \frac{1}{1000}, \tag{2}$$

Probability that 1000 MC iterations will not be the 0.001 event

$$= \left(1 - \frac{1}{1000}\right)^{1000}, \tag{3}$$

Probability that 1000 MC iterations give atleast one 0.001 event

$$= 1 - \left(1 - \frac{1}{1000}\right)^{1000} = 0.6323 = 63.23\%. \tag{4}$$

For 1000 MC iterations, the probability that at least one 1/1000 event occurs is only 63.23%. Hence, applying 1000 iterations will not give an accurate estimate of the underlying statistics of the distribution at a 0.001 resolution. We therefore propose a formula that gives the lowest possible number of iterations to perform for an accurate representation of the underlying statistics at the required resolution when combining the MC approach with FDR. It is analogous to probability with replacement, with the FDR equation for the first sorted *p*-value substituted for the 1/1000 chance event (the FDR equation gives the desired resolution level for accurate statistics). The new equation is also set equal to 1 to indicate that the statistics at the desired level of resolution should be achieved 100% of the time when the number of iterations is optimized:

$$1 - \left(1 - \left(\frac{1}{N} \cdot \alpha_{FDR}\right)\right)^{\text{Iterations}} \approx 1. \tag{5}$$

Evidently, the equation above can only be approximately fulfilled, as it converges as number of iterations goes to infinity:

$$\lim_{\text{Iterations}\to\infty} \left(1 - \left(\frac{1}{N} \cdot \alpha_{FDR}\right)\right)^{\text{Iterations}} = 0. \tag{6}$$

The right side of the equation can be replaced by E_A, symbolizing an error in accuracy. Then applying the natural logarithm

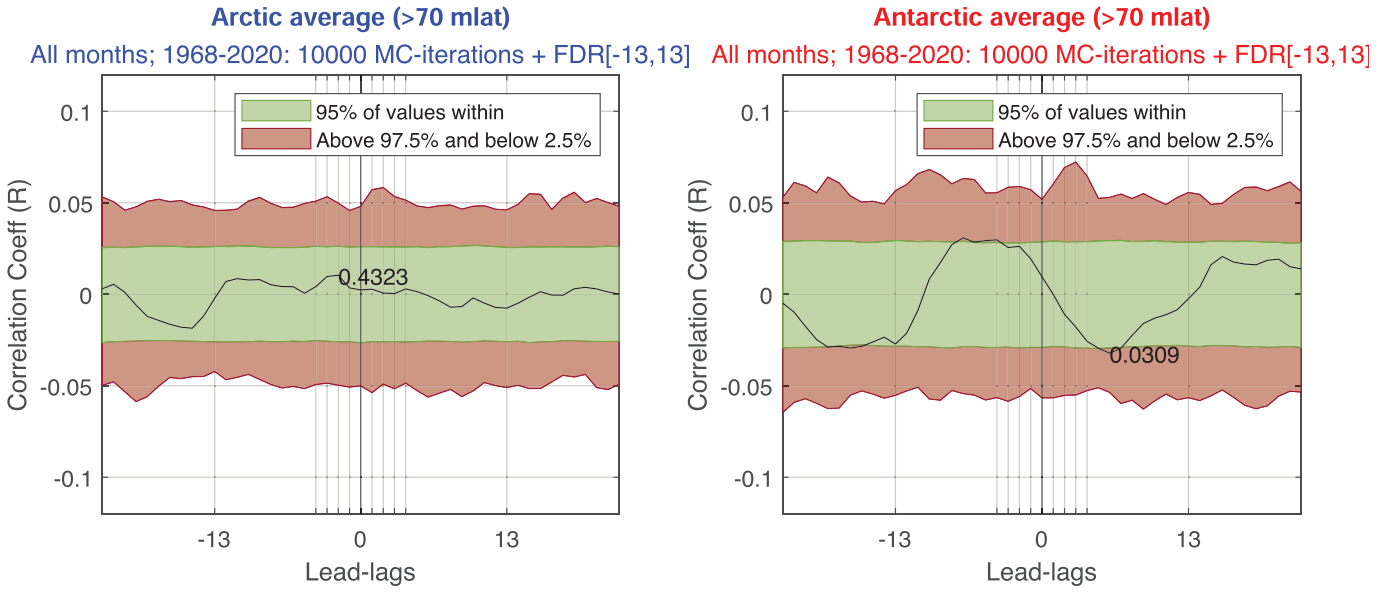

Fig. 4. *Left panel*: The significance level for the time-lagged cross-correlation after 10,000 MC-iterations for the period 1968–2020 in the NH. FDR interval is set between lead and lag −13 to +13. *Right panel*: Same procedure, only for the SH. No significance is obtained in either hemisphere. The smallest *p*-value obtained from the MC simulation is highlighted at the point of occurrence. This routine will be done for every figure for comparison.

on both sides, the equation gives the number of iterations required to achieve the desired error in accuracy when representing the underlying statistics at a given resolution:

$$\text{Iterations} = \frac{\ln(\mathrm{E}_A)}{\ln\left(1 - \left(\frac{1}{N} \cdot \alpha_{\mathrm{FDR}}\right)\right)}. \tag{7}$$

For our cases, where most time-lagged cross correlation plots consist of 41 lead-lags, $\alpha_{\mathrm{FDR}} = 0.09$, and by setting $E_A = 10^{-9}$ ($E_A = 10^{-9}$) indicates there is a 1 in a billion chance of not obtaining an accurate representation of the underlying statistics at the desired resolution), the equation yields:

$$\text{Iterations} = \frac{\ln(10^{-9})}{\ln\left(1 - \left(\frac{1}{41} \cdot 0.09\right)\right)} = 9430. \tag{8}$$

This implies that >9430 iterations will ensure that our specified resolution of (1/41)·0.09 = 0.0022 will be fulfilled with a 99.9999999% accuracy. The following analyses apply significance assessments based on 10,000 MC iterations.

3 Analyses and results

3.1 Full data period 1968–2020

The time-lagged cross correlation between the IMF B_y and the geopotential height $Z_{g(\mathrm{NH})}$ and $Z_{g(\mathrm{SH})}$ is calculated from 1968 to 2020. As seen in Figure 4, no significance is obtained in either hemisphere by applying MC simulation and FDR significance tests for the interval −13 to +13. However, the SH exhibits a peak in the correlation values from lead-lag −8 to −2.

3.2 Seasonality analysis

The next step is to look for potential seasonal dependency. The atmosphere exhibits large variability depending on the seasons, which again could lead to different pathways and strengths of the coupling between IMF B_y and the polar surface pressure. The full data period is therefore sorted into the seasons grouped as December, January, February (DJF), March, April, May (MAM), June, July, August (JJA), and September, October, November (SON). The time-lagged cross-correlation analysis is then performed for each season individually, with the results shown in Figure 5. In the NH, a significant positive anomaly occurs around lead-lag −4 for the MAM period (which is significant even after the FDR method). The same positive anomaly, shown in Figure 4, still occurs in the SH for both MAM and JJA but is not significant with FDR interval −13 to +13 lead-lags. The Mansurov effect should impose opposite responses in the ionospheric polar cap for the two hemispheres. Positive anomalies are expected in the SH and negative anomalies in the NH at lead-lag 0 and beyond. A general overview of the responses seems more in-phase than out-of-phase for our results. In line with previous studies the seasonal analysis in this section, as well as a sector structure analysis (Sect. 3.5) and combined seasons and sector structure analysis (Sect. 3.6) are also performed for the most cited period of 1999–2002. In summary, there is no season or sector structure rendering statistical significance for the 1999–2002 period after the FDR method is applied. Plots for this sub-period can be found in the Appendix.

3.3 Sector structures

Structures in the solar wind originate from two mechanism. Structures are either imposed from the Sun directly, or, structures form as the solar wind propagates outwards and fills the

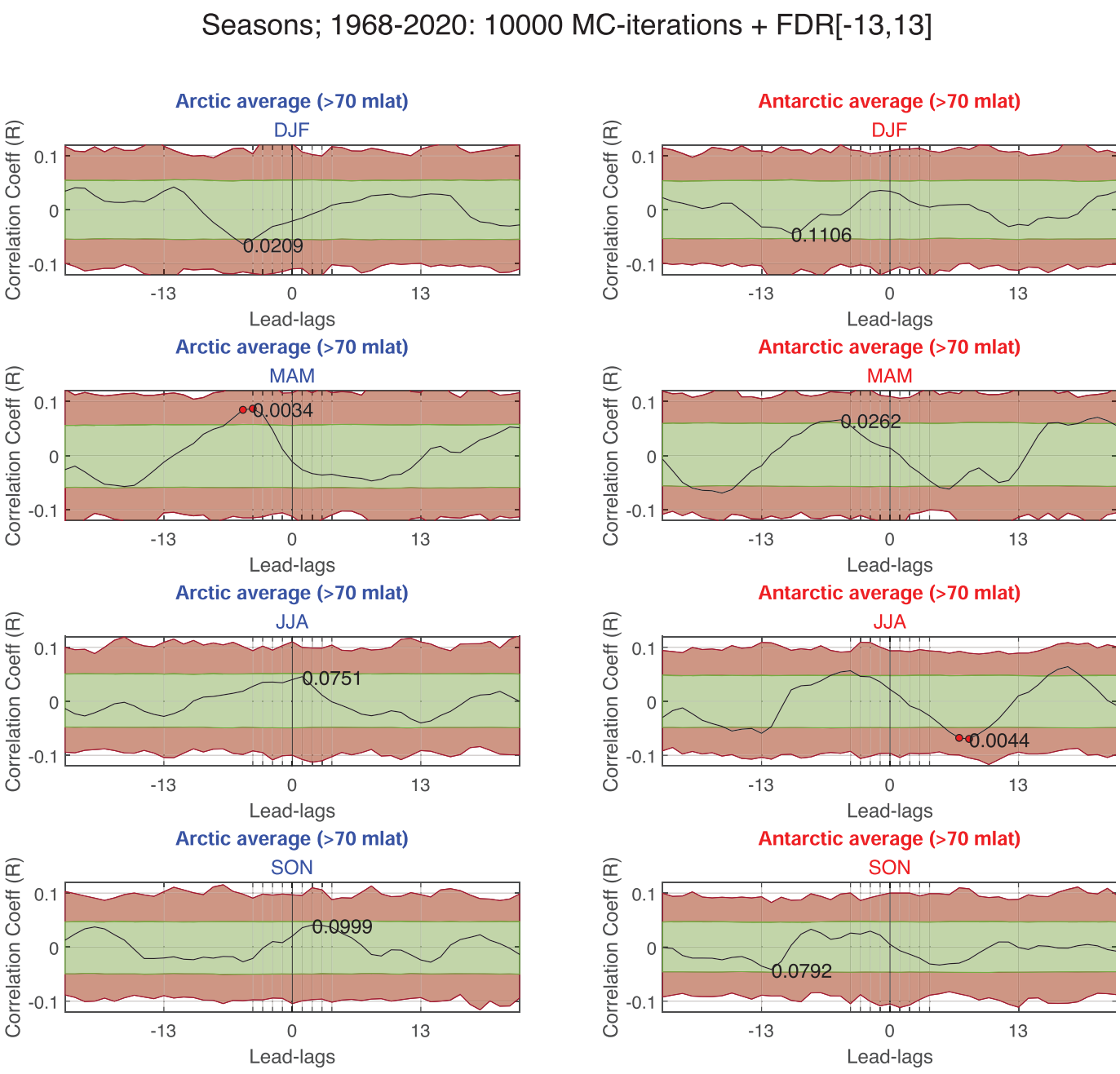

Fig. 5. *Left panels*: The significance level for the time-lagged cross-correlation after 10,000 MC-iterations for the period 1968–2020 in the NH for the months DJF (top panel), MAM (middle top panel), JJA (middle bottom panel) and SON (bottom panel). FDR interval is set between lead and lag −13 to +13. Statistical significance after the FDR method is observed in MAM at lead-lag −4 in the NH and in JJA at lead-lag 7 in the SH. *Right panels*: Same procedure, only for the SH. No significance is observed after the FDR method.

heliosphere (Viall et al., 2021). The global solar magnetic field itself is composed by a superposition of the dipole, quadrupole and octupole harmonics, which can lead to imposed 2-, 4- and higher order harmonic sector structures. Tinsley (2022) specifically highlights the importance of the 2-sector solar wind structures in regards to the Mansurov effect, and hypothesise that this sector structure favors the Mansurov effect compared to 4-sector or irregular sector structures. The distinction of the two solar wind sector structures are illustrated in Figure 6. In the left panel, the dipole harmonics of the global solar magnetic field dominates, and the away and toward sectors experienced on Earth will oscillate with a periodicity of approximately 27-days. Tinsley (2022) hypothesises that longer duration of 2-sector structures nudges uncorrelated pressure oscillations into partial synchronization with the solar wind, while due to the more irregular nature, this is not accomplished for the 4- or irregular sector structures illustrated in the right panel. The frequently cited period 1999–2002 has a 68% occurrence rate of

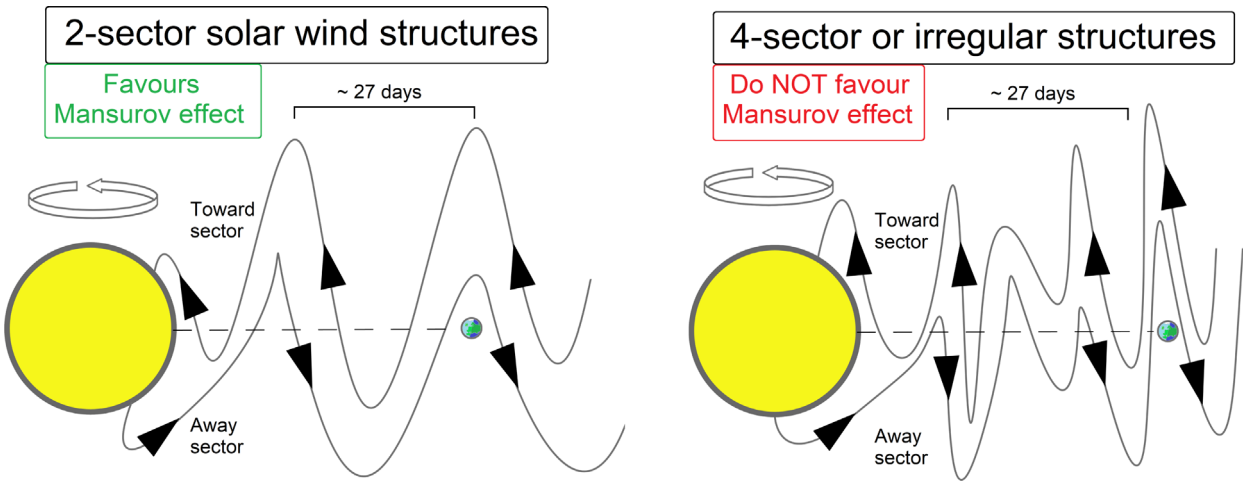

Fig. 6. *Left panel*: Illustration of 2-sector solar wind structures. The sector structures oscillate with a periodicity of approximately 27 days. *Right panel*: 4-or irregular sector structures. The sector structures oscillate with either a ~13.5 day periodicity, or irregular periodicity.

the 2-sector structure pattern (Tinsley, 2022). These numbers were manually identified by Tinsley (2022), which recommends a wavelet analysis for more accurate and objective identification.

The middle panel of Figure 7 shows the scalogram obtained by wavelet analysis of the B_y-index, while the top panel shows the raw B_y-index with red lines indicating a 2-sector structure, and blue lines indicating 4 or irregular sector structures.

The analysis itself is done by binning all days with the largest intensity in the scalogram of a period occurring in the interval between 22 and 32 days as a 2-sector structure, while the remaining days are binned as 4 or irregular sector structures. From the wavelet analysis, we find a 73% occurrence rate of 2-sector structures and a 27% occurrence rate for 4 or irregular sector structures in the 1999–2002 period. Tinsley (2022) state that the period 2007–2010 yields a less impactful Mansurov effect as the occurrence rate of 2-sector structures is only 40%. However, the wavelet analysis suggests a 65% occurrence rate of the 2-sector structure for this period. Figure 7 also provides the yearly occurrence rate for the period 1968–2020 of 2-sector structures obtained from the scalogram (bottom panel).

3.4 Time-lagged cross-correlation and the dependence on the autocorrelation function of both the forcing and responding variable

Before dividing the IMF B_y data into the two different sector structures, a clear understanding of the inner workings of the time-lagged cross-correlation method is needed.

Figure 8 shows a power spectrum analysis (left panels) of the IMF B_y, the autocorrelation function for $Z_{g(\mathrm{NH})}$ (middle panels) and the autocorrelation for $Z_{g(\mathrm{SH})}$ (right panels). The analysis is also divided into 2-sector structures (top panels) and 4- or irregular sector structures (bottom panel). The top left panel shows that there is a clear peak in power surrounding 27 days/cycle, which is expected as the 2-sector structures exhibit a 27-day periodicity on average. In the bottom left panel, a clear peak in power is seen around 13.5 day/cycle, which is also expected as the 13.5 periodicity is the second most dominating sector structure. For the autocorrelation functions of the geopotential height, not much variance is seen by the sector division. The NH and SH exhibit similar autocorrelation functions.

Edvartsen et al. (2022) shows how a periodic forcing variable together with an autocorrelated response variable is susceptible to producing artificial periodic responses when a time-lagged cross-correlation method is used. Here, we demonstrate further implications of this artificial anomaly which is particularly relevant in the investigation of the Mansurov effect, but also generally in any other phenomenon with a periodic forcing and autocorrelated response variable.

The left column of Figure 9 shows 1000 iterations where the IMF B_y is firstly divided into 2- and 4- or irregular sector structures before it is cross-correlated with the geopotential height data series $Z_{g(\mathrm{NH})}$. (Due to the roughly similar autocorrelation functions for the hemispheres, it is only necessary to show this experiment for one hemisphere, where the choice of NH is arbitrary.) For every iteration, the geopotential height data series are phase-randomized. In essence, this is the same process that defines the significance limits in the figures above (Figs. 4 and 5). In the middle column, the largest positive peaks occurring between day −13 and +13 for every iteration are shifted and placed at day 0. At last, the right column shows the averaged response of the shifted peaks shown in the middle panels. It is evident that the 2-sector structure in both hemispheres (1. and 3. row) produces a larger artificial periodicity than the 4- or irregular sector structure (2. and 4. row). Simply put, this means that any time-lagged cross correlation between the IMF B_y and the geopotential height in 2-sector structure periods will have higher values in general, as compared to the 4- or irregular sectors structures. These higher values are then only a result of the autocorrelation function of the forcing and responding variable. The same experiment is performed on the raw geopotential height data in both hemispheres for the period 1968–2020 with similar results.

In addition to being dependent on the autocorrelation function of the forcing and response variables, the value of the correlation coefficient will also depend on the amount of data points used. This highlights the need for modern statistical methods such as MC simulation. MC-simulations applied on suitable statistical material (phase-randomization of original

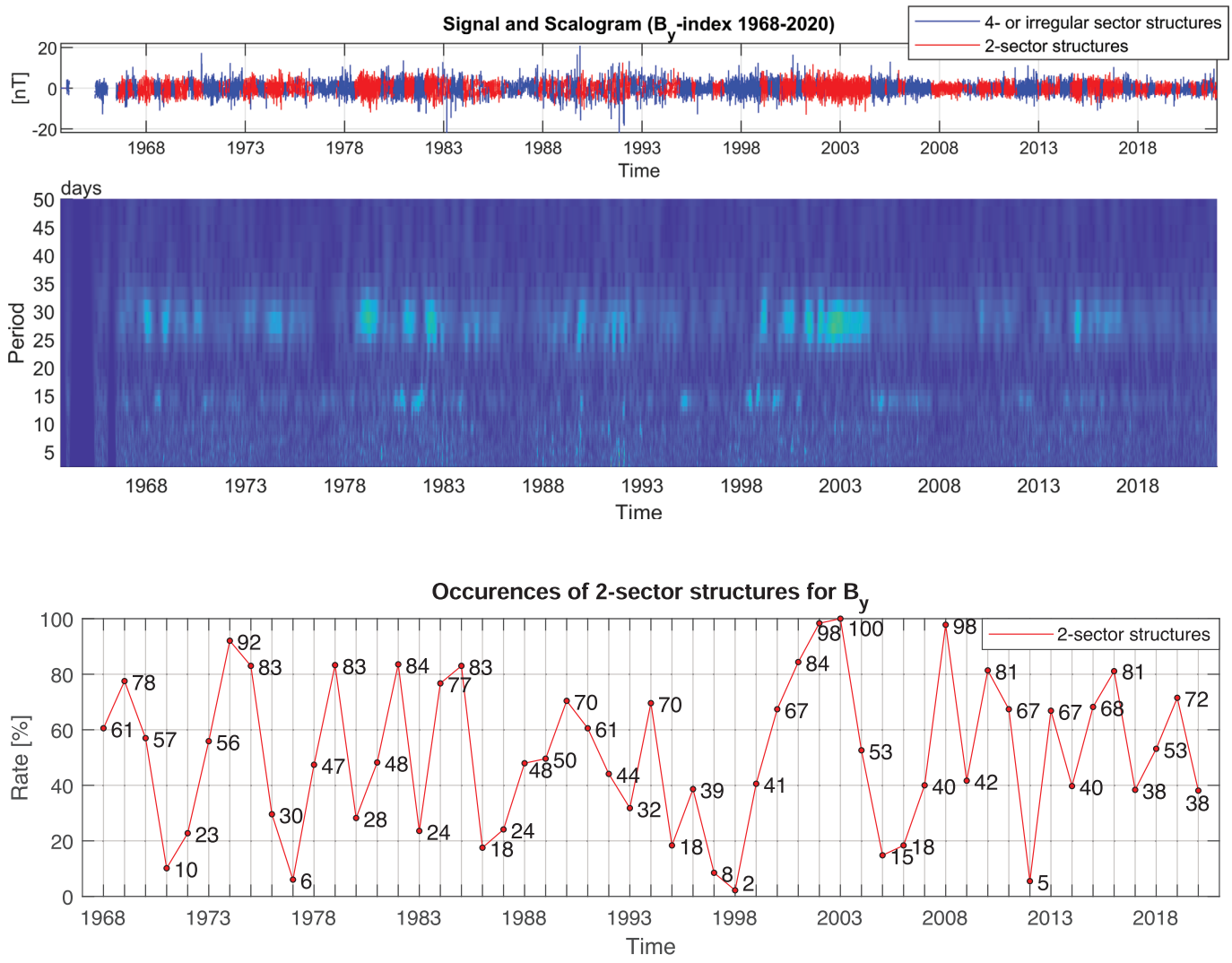

Fig. 7. *Top panel*: The B_y-index over the time period 1968–2020. Red mark periods of 2-sector structures, while blue mark periods of 4-or irregular sector structures. *Middle panel*: Scalogram obtained by a wavelet analysis of the B_y-index over the same time period. The dominating frequencies can be seen by the lighter color bands around 13.5 and 27 days per period. *Bottom panel*: Yearly occurrence rate of 2-sector structures for the B_y-index over the same period.

response data series) will take all the relevant information affecting the correlation analysis (autocorrelation of forcing and response variable, and amount of data points) into account. This will result in a realistic p-value that is of higher relevance than the correlation values itself.

3.5 Sector structures analysis

The time-lagged correlation analysis sorted by solar wind sector structures for the full-time period 1968–2020 is performed. Figure 10 shows the time-lagged cross correlation between the IMF B_y and the variation values $Z_{g(\mathrm{NH})}$ and $Z_{g(\mathrm{SH})}$ for periods of 2-sector structures (top panels) and periods of 4- or irregular sector structures (bottom panels). No clear response is seen in the NH for any of the sector structures over the whole data period. However, for the SH, the 2-sector structures seem to enhance the peak in pressure around day −6 compared to Figure 4 where sector structures are not taken into account. It is noted that the positive anomaly is still not statistically significant after applying the MC simulation together with the FDR method for the interval −13 to 13. The timing of the positive response on day −6 is not in line with the current Mansurov hypothesis, where the pressure anomaly should lag the IMF B_y driver by a few days (Frederick et al., 2019; Tinsley et al., 2021). We also note that different magnitudes are seen for the significance intervals (green and red shaded area) between the results from the 2-sector structures and 4- or irregular structure analysis even though the two-sector structures have approximately the same number of data points. This is a consequence of the effect described in Section 3.4, demonstrating the importance of MC simulation when assessing the statistical significance.

3.6 Seasons and sector structure analysis

The final step investigates the combination of both seasonal and sector structure dependence. The results are shown in Figure 11. In the first column, the time-lagged cross-correlation

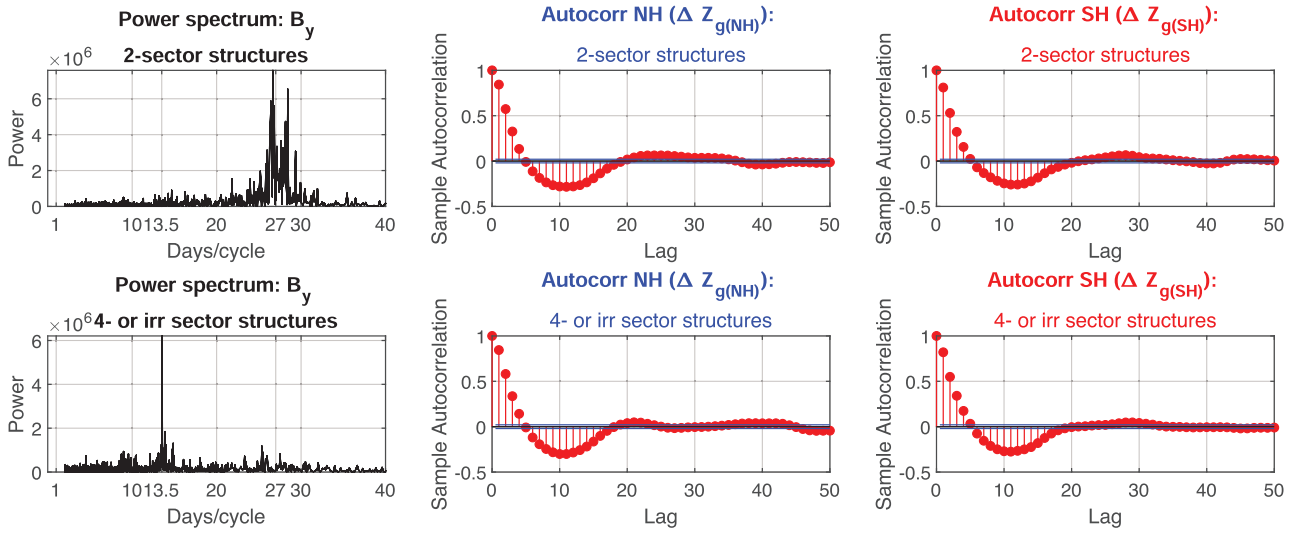

Fig. 8. *Left panels*: Power spectrum of the B_y-index over the time period 1968–2020 for 2-sector structures (top panel)/4- or irregular sector structures (bottom panel). *Middle panels*: Autocorrelation function of the geopotential height ($Z_{g(\mathrm{NH})}$) over the same period in the NH for the 2-sector structures (top panel)/4- or irregular sector structures (bottom panel). *Right panels*: Autocorrelation function of the geopotential height ($Z_{g(\mathrm{SH})}$) over the same period in the SH for the 2-sector structures (top panel)/4- or irregular sector structures (bottom panel).

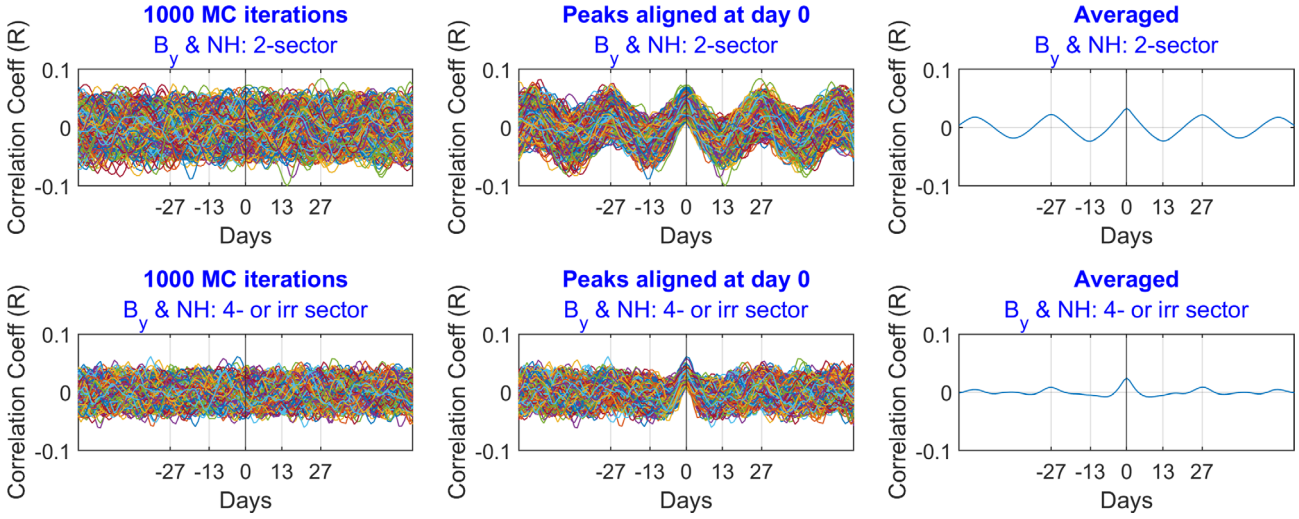

Fig. 9. Full data period 1968–2020 divided into the different sector structures *Left panels*: 1000 MC iterations where the correlation coefficients are calculated between the B_y-index and the phase randomized $Z_{g(\mathrm{NH})}$ data series for the 2-sector structures (top panel)/4- or irregular sector structures (bottom panel). *Middle panels*: All 1000 individual results of the MC-iterations from the left panels aligned such that the maximum value within −13 to +13 is projected to day 0. *Right panels*: Averaged response of the middle panel. Note the large difference between the 2- and 4-sector structure periods.

for the four different seasons in the NH for 2-sector structures is shown, and 4- or irregular sector structures are shown in the second column. The third and fourth columns follow the same logic for the SH. In all plots, the FDR interval is set from lead −13 to lag +13. The highest obtained significant data point is also marked with its corresponding *p*-value.

As a general overview, there exists no combination of sector structure and season obtaining significant data points in line with the current Mansurov theory (a positive significant anomaly around day 0 in the SH, and a negative significant anomaly around day 0 in the NH). In DJF, the responses in both hemispheres do follow this pattern. For the NH, this fits the correlations found by Zhou et al. (2018) and Tinsley et al. (2021) predicting a local winter effect, but does not fit with the theory in the SH. It is noted that these correlations are still not statistically significant. However, the same reoccurring pattern of a positive pressure anomaly in both NH and SH around lead-lag −5 appears in March, April and May (MAM) for the 2-structure periods, and renders statistically significant in the SH. It also appears in JJA (mostly in the SH).

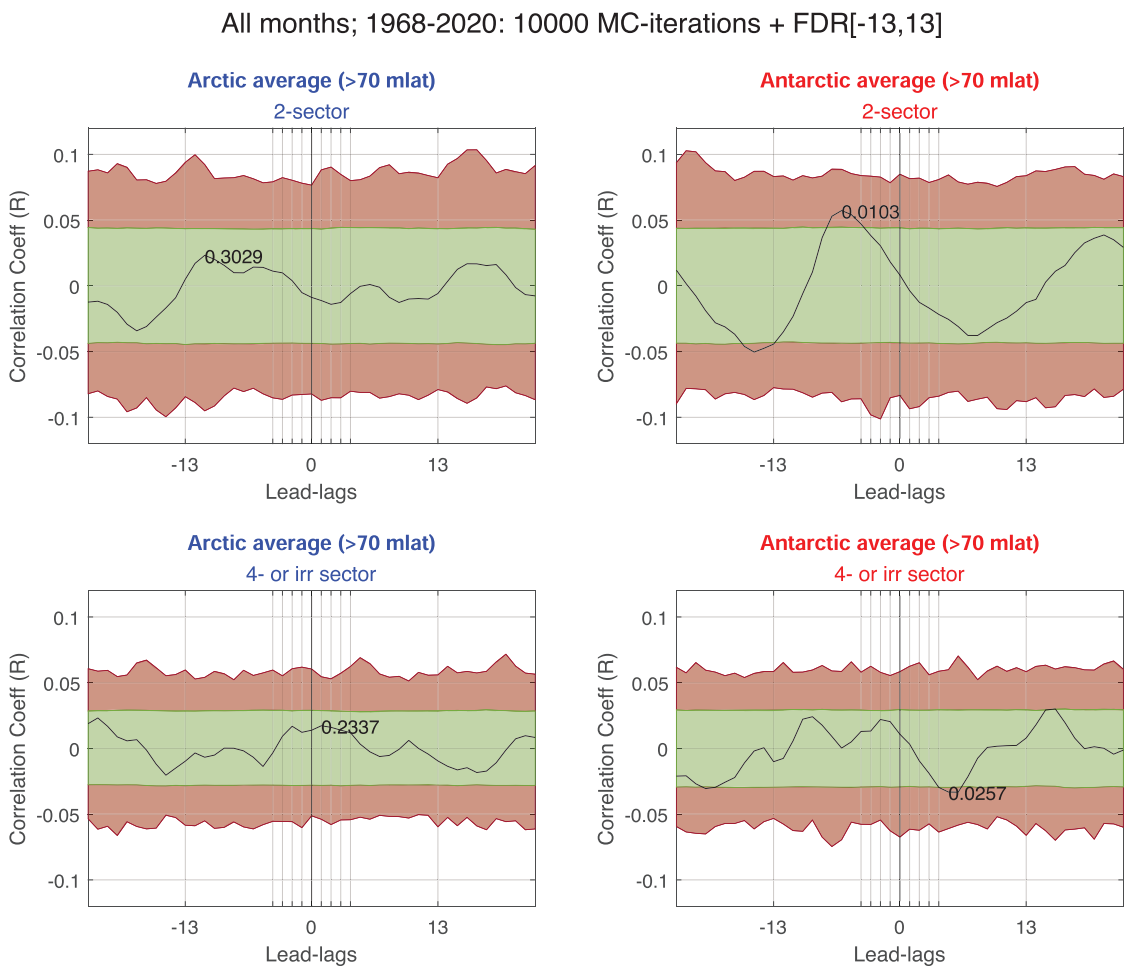

Fig. 10. *Left panels*: The significance level for the time-lagged cross correlation after 10,000 MC-iterations for the period 1968–2020 in the NH for 2-sector structures (top panel)/4- or irregular sector structures (bottom panel). FDR interval is set between lead and lag −13 to +13. *Right panels*: Same procedure, only for the SH. No significance is obtained in either hemisphere.

3.7 Day −5 anomaly

From all the analyses no indication of the Mansurov effect is found. However, the work has unraveled a rather strange occurrence. In Figure 11, where atmospheric seasons and solar sector structures are combined, a positive anomaly around day −5 is seen concentrated around MAM in both hemispheres for the 2-sector structure periods. This same anomaly is also present in the SH in Figure 10 when divided according to the 2-sector structures for all months. In Figure 5, the anomaly is even statistically significant in the NH for MAM after the FDR method is applied, and it is present in Figure 4 in the SH for the full data period with no sorting requirements. Summarized, our analyses have unveiled a reoccurring positive pressure anomaly happening on average 5 days before the peak B_y anomaly in both hemispheres. The anomaly obtains the highest statistical significance in MAM but is also visible in JJA in both hemispheres. For division into sector structures, the anomaly favors the 2-sector structure in both hemispheres.

As the anomaly is most persistent in both hemispheres in the 2-sector structure in MAM, the latitudinal extension at this specific lead lag is explored. Figure 12 shows the zonal mean pressure differences ($Z_{g(\mathrm{SH})}$ and $Z_{g(\mathrm{NH})}$) on lead −5 for days with $B_y > 3$ nT averaged and subtracted the average of days with $B_y < -3$ nT (note that correlation is not used, but rather a double superposed epoch analysis. This is done for coherence with earlier analyses on the Mansurov effect (see Zhou et al., 2018, Figs. 1–3). As an extra fail-proof for the significance assessment, we have run the MC simulation for 1,000,000 iterations, including the FDR method over all latitudes giving a total of 72 data points. We note that the FDR over all latitudes may not be physically justified, as the Mansurov effect is only expected to occur at high latitudes. However, since day −5 is a rather unknown anomaly, the latitude-wise extension is also unknown. With all latitudes included, one will therefore expect less significance at the 95% level than if the FDR method only covered the poles. Nevertheless, the figure still demonstrates a remarkable statistical result. The pressure response is significant from 85 to 90° S and 70 to 90° N, where the latitudes 75 to 80° N have a positive response outside of both tails of the probability distribution. In reality, this means that these data points have a p-value less than 0.000001.

3.8 Heliospheric current sheet crossings

To further investigate the reality of the day −5 anomaly, a final analysis focusing on heliospheric current sheet crossing events (HCSC) is performed. HCSC marks the intersection

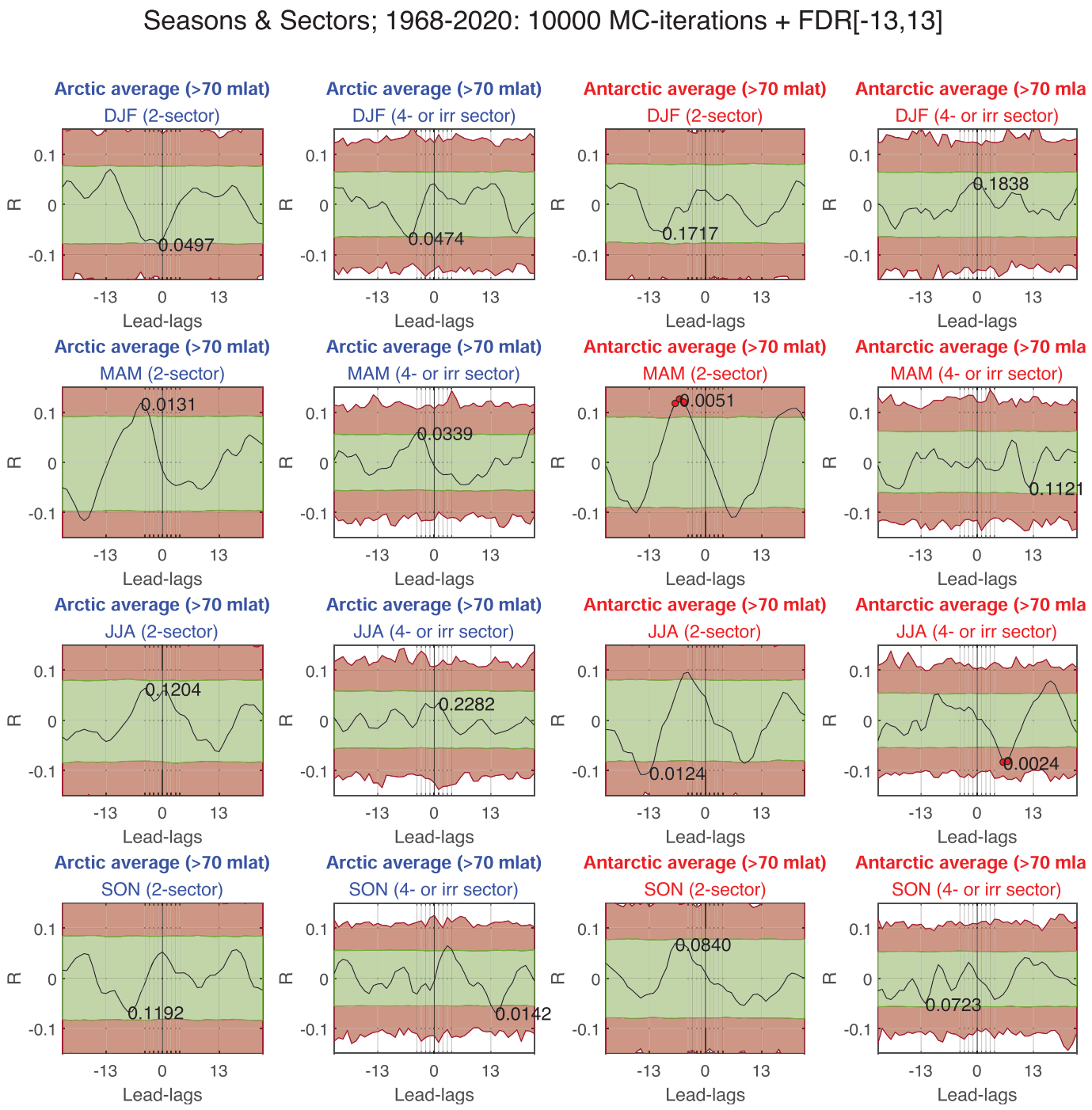

Fig. 11. *Left panels*: The significance level for the time-lagged cross-correlation after 10,000 MC-iterations for 2-sector structures in the period 1968–2020 in the NH for the months DJF (top panel), MAM (middle top panel), JJA (middle bottom panel), and SON (bottom panel). FDR interval is set between lead and lag −13 to +13. *Left middle panels*: Same procedure for the 4- or irregular sector structures in the NH. *Right middle panels*: Same procedure for the 2-sector structures in the SH. *Right middle panels*: Same procedure for the 4- or irregular sector structures in the SH.

between the toward sector ($B_x < 0$, $B_y > 0$) (T) and the away sector (A) ($B_x > 0$, $B_y < 0$) of the IMF. As the magnetic field flips, there is an increase in proton density, proton dynamic pressure, magnetic field intensity, and a decrease in solar wind speed (Kan & Wu, 2021). Crossing events happen in between the maximum B_y events, which could mean that the day −5 anomaly observed fits with the time of the crossing. A list of crossing events derived by Prof. Leif Svalgaard[1] spanning the data

[1] https://svalgaard.leif.org/research/sblist.txt

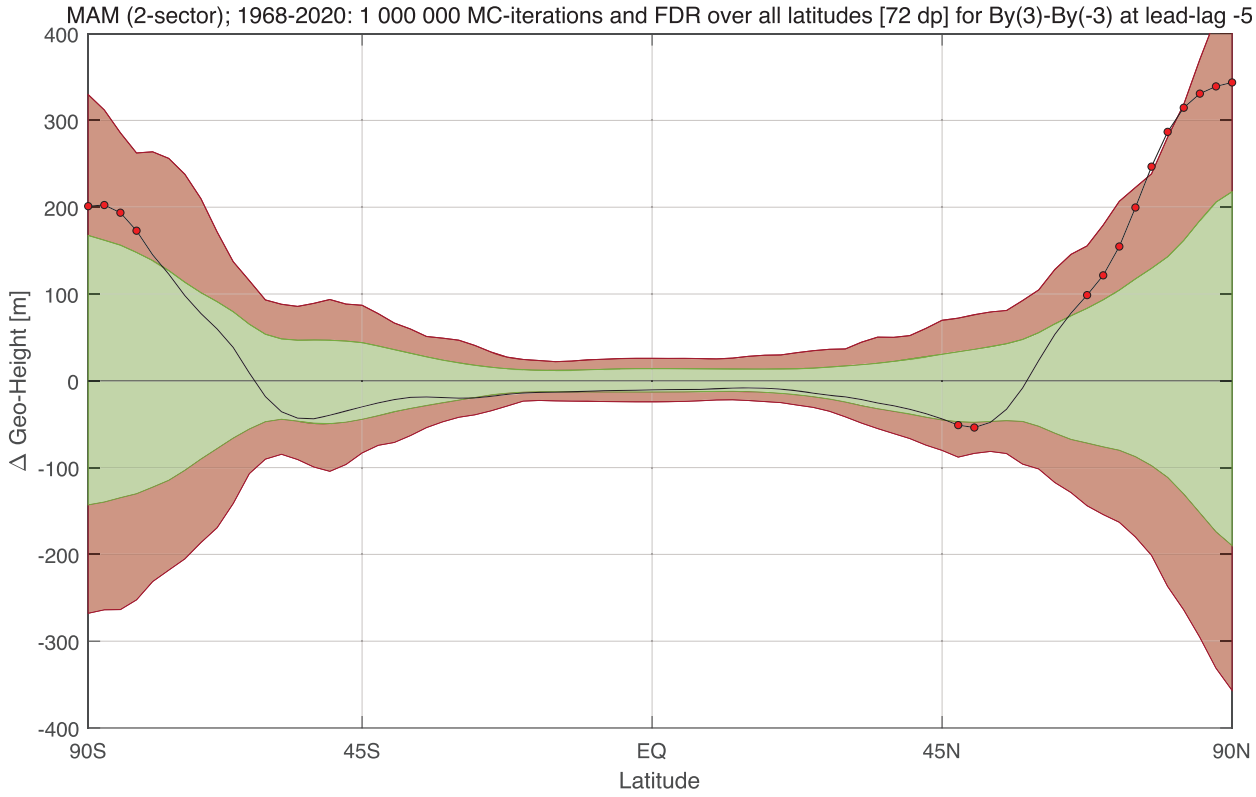

Fig. 12. The significance level for the superposed epoch analyses of zonal means after 1,00,000 MC-iterations for 2-sector structures in MAM for the period 1968–2020. Latitudes 75–80° N renders a *p*-value less than 0.000001 as the positive anomaly has an absolute value outside both tails of the distribution

interval 1968–2020 is applied. Since MAM without the sector structure sorting is the result with the highest significance for the lead-lag plots, we will focus on this period. Sector structure sorting for the HCSC will be considered in the discussion.

Figure 13 shows superposed epoch analyses of the HCSC for MAM over the whole data period 1968–2020. Similar significance assessment as other lead-lag plots apply. The top row shows the results when the pressure on days with "A T" sector crossings are averaged, and subtracted the average pressure on days with "T A" sector crossings. The middle row shows the superposed epoch for only days where an A sector crossing occurs, while the bottom row shows a superposed epoch for only days where a T sector crossing occurs. As seen in the figure, when the two different crossings are combined as seen in the top row, we get a statistically significant positive anomaly in the NH peaking at day −2. Comparing it to Figure 5, the significance is increased for the crossings compared to the correlation with B_y. For the SH, no significance is obtained. In the middle and bottom rows, where the different crossings are treated separately, significance is obtained in the NH for A → T crossings.

Not shown is the same seasonal analysis for HCSC, also including the separation of sector structures, equivalent to Figure 11. The most significant response for the NH is seen in the 4- or irregular sector structures, and not the 2-sector structures which show the most significant response when B_y is correlated to the pressure. In the correlation analysis, (ex. Fig. 11), emphasis is put on the highs and lows of B_y. In the superposed epoch analysis of crossings, every event is treated equally, and the average response of all events is shown. As any mechanism for the HCSC affecting the polar surface pressure is yet to be determined, we can not know if the most impactful HCSC is related to times with the largest variations of B_y. If we assume that the significant correlations seen for the B_y and pressure (Figs. 5 and 11) are in reality anomalies resulting from HCSC (Fig. 13), a non-linear relationship between the strength of the B_y and the surface effect of a HCSC could result in differing signal strengths between the two modes of analysis. We also note that analyzing the zonal mean differences of the HCSC (equivalent to Fig. 12) results in the 4-sector structure showing anomalies outside of the probability distribution in the NH at day −2.

In general, the HCSC superposed epoch analysis has shortcomings in terms of the timing of the response. The peak anomaly in the NH occurs 2 days before the actual event happens, and no significant response is seen in the SH. However, the responses seen are statistically significant, and one can argue that the pressure response is closer to a physically justified response.

4 Discussion and possible hypotheses

In previous work, the Mansurov effect is shown to not be statistically significant on the decadal timescale (Edvartsen et al., 2022). The same study also shows how previous evidence for the Mansurov effect (27-day cyclic pressure response) is due to a statistical bias created by a periodic forcing and a temporally autocorrelated response variable, and cannot be treated

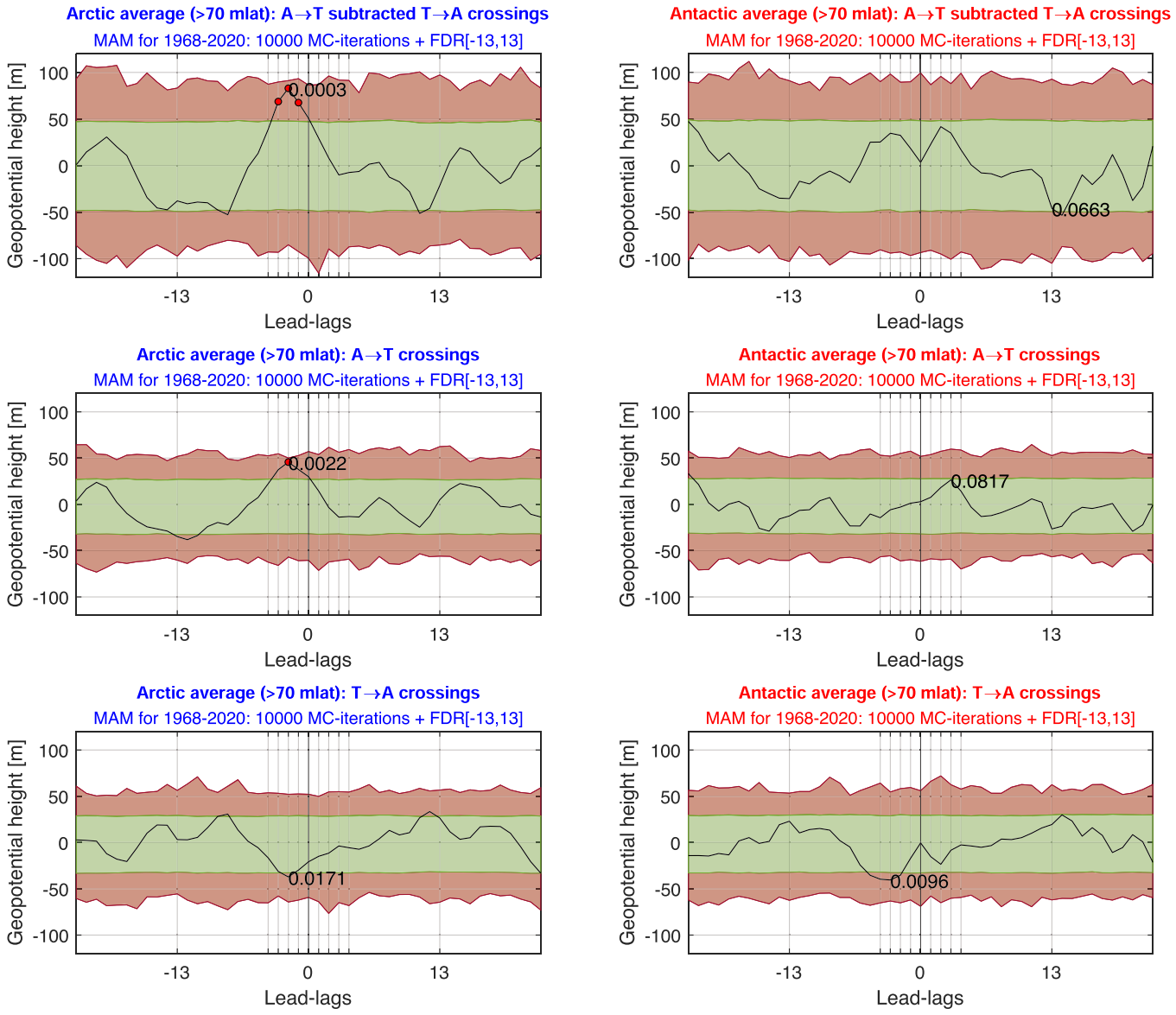

Fig. 13. *Left panels*: The significance level for the superposed epoch analyses of HCSC in MAM for the period 1968–2020 in the NH. The top panel show "A T" events subtracted "T A" events. The middle panel shows only "A T" events, while the bottom panel shows only "T A". *Right panels*: Same procedure, only for the SH. Statistical significance after FDR is found in the NH when looking at the difference between the asymmetric events (top left panel) and for only the A→T events (middle left panel).

as evidence for a physical link. This evidences weakens the overall case for the Mansurov effect, as the hypothesis itself is built from pure correlation analyses (Mansurov et al., 1974; Burns et al., 2008; Lam et al., 2013, 2018; Zhou et al., 2018; Tinsley et al., 2021). However, Edvartsen et al. (2022) did not consider in depth the possibility of seasonal and solar wind structure dependence, which is the aim of the current study.

This study includes a seasonal analysis of decadal timescales. When analyzing seasonal variations, this considers both the atmospheric state and the Earth's dipole tilt relative to the IMF, which affects geomagnetic activity. Local winter months lead to stronger polar vortexes, and higher atmospheric variability, while less variability and weaker vortexes are seen in local summer. In the solar wind, different seasons mean different geometric conditions impacting the connection between the IMF and Earth's magnetic field. This manifests itself as the Russel McPherron effect, which is the increased probability of a negative B_z-component leading to increased geomagnetic activity occurring around early April and early October (Russell & McPherron, 1973). By dividing the time period 1968–2020 into DJF, MAM, JJA, and SON we show (Fig. 5) that none of the specific seasons produce a significant response in line with

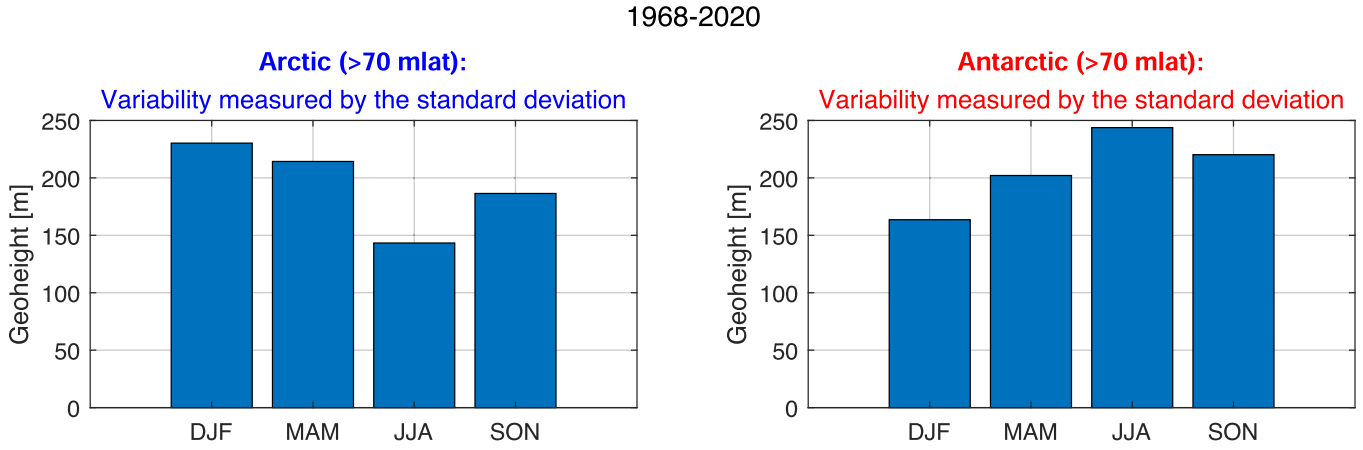

Fig. 14. Variability in $Z_{g(\mathrm{NH})}$ and $Z_{g(\mathrm{SH})}$ measured by the standard deviation of the different seasons. Largest variability is seen in the local winter.

the Mansurov hypothesis. However, a significant positive pressure anomaly occurs around lead-lag −5 in the NH for MAM, with 3 data points rendered statistically significant after MC-simulations and FDR-method over the interval −13 to 13 lead-lags. Though not significant according to the FDR method, the SH does show phase coherence with the NH for the MAM period. From the perspective of the Mansurov hypothesis, the peak pressure perturbation is expected to happen days after the forcing. This is due to the microphysical changes being small and acquiring time to materialize as macro-physical changes in cloud radiative properties (Frederick et al. 2019; Tinsley et al., 2021). In conclusion, an effect occurring 5 days before the forcing is unphysical given the Mansurov hypothesis. Considering the significant period of MAM, this might be linked to the Russel–McPherron effect, which states that in these months, the connectivity between the IMF and Earth's geomagnetic field increases. This could be hypothesized to lead to the enhanced surface impact of any mechanism propagating from the solar wind to the surface. However, it would then also be reasonable to expect a pressure response around late September/early October, which is not observed in our results. Another way the atmospheric variability could play a role is if the effect is very small, and risks being disguised by background noise. Figure 14 shows the standard deviation of $Z_{g(\mathrm{NH})}$ and $Z_{g(\mathrm{SH})}$ as bars, for the specific seasons analyzed in this study. The local summer in both hemispheres has the least variability. However, the lowest p-values are obtained in MAM. In NH, this is the month with the second-largest pressure variability. On this basis, it is not likely that the atmospheric variability acts as an obscurer for an effect that is always occurring. Earth's dipoles' geometrical positioning or specific reoccurring atmospheric seasonal conditions increasing the coupling between IMF and the polar atmosphere might rather be at play. There have been studies showing that winters following volcanic eruptions, which inject large quantities of sulfate aerosols into the stratosphere, increase the correlation between solar wind parameters and atmospheric effects (Tinsley et al., 2012; Zhou et al., 2014). This effect is not taken into account in this study and remains an open pathway for further research.

Moreover, our study includes the division of the IMF into either 2-sector or 4- or irregular sector structures. These sectors are defined according to the periodicity of the fluctuating B_y, with 2-sector structures defined as a 27-day cycle, and 4- or irregular sector defined as 13-day and all other cycles occurring (Power spectrum of the two distinct sectors for the IMF B_y can be seen in Fig. 8). Previous research has highlighted the 2-sector structure as important for the manifestation of the Mansurov effect, with the argument mainly based on the occurrence rate in the regularly studied period of 1999–2002 (Tinsley, 2022). It is hypothesized that a continuous period of 2-sector structure oscillations with large amplitude jumps in the B_y (>6 nT) is needed to nudge the internal atmospheric waves into partial phase coherence (from now called the B_y Nudge hypothesis). However, Tinsley (2022) also states that the period 2007–2010 does not yield a correct Mansurov manifestation due to the low occurrence of 2-sector structures (40%). As we see in Figure 4, our results show that the period 2007–2010 has as high as a 65% occurrence rate of the 2-sector structure. Nevertheless, as the 2-sector structures in the 2007–2010 period do not reach as high peak amplitudes as the 1999–2002 period, this might still be applied in favor of the B_y Nudge hypothesis. Figure 4 reveals that if this is the condition necessary for the manifestation of the Mansurov effect, there exists no other sub-period in the interval 1968–2020 having as high amplitudes and long duration of 2-sector structures as the period 1999–2002. Hence, in case the hypothesized pathway does exist, it is likely to excerpt a negligible role with respect to climate variability on decadal scales. This is supported by our analysis of the correlation between the B_y and pressure after the sector division, as seen in Figure 10. As our results show, the sector division does not enhance any response associated with the current Mansurov theory. It does, however, enhance the day −5 anomaly in the SH. Compared to Figure 4, which is the full-time period, the sector structure division lowers the p-value for the day −5 anomaly substantially in support of favorable 2-sector structures in the IMF.

The final step in this study includes both seasonal and sector structure divisions. The results are shown in Figure 11. None of the combinations show a response in either hemisphere that is in line with the current Mansurov theory. However, for the day −5 anomaly pattern, both MAM and JJA show phase coherence in both hemispheres for the 2-sector structures. In the NH, MAM and 4- or irregular sector structures also show phase coherence, but with less significance than the 2-sector. As stated early, none

of the combinations show a signal that is significant at the 95% level after considering MC-simulation and FDR-method for the interval −13 to +13 lead-lags.

This study aims to unravel any seasonal or solar wind sector structure dependence on the Mansurov effect, as this was an open end in our earlier study (Edvartsen et al., 2022). For the main known arguments about specific dependencies, mainly seasonal and IMF structural effect, no results obtained show the existence of a significant correlation between the pressure in either hemisphere and the IMF B_y, acting according to the hypothesized mechanism. The study is not able to conclude that such a pathway does not exist, only that the data used in our study does not support it. However, in this process, the analyses have unraveled a rather strange but persistent occurrence, namely the day −5 positive peak anomaly occurring in both hemispheres mostly in the MAM period and the 2-sector solar wind structure. The anomaly is persistent and also renders significant values for some of the analyses after FDR. Figure 12 shows the zonal mean pressure with respect to days for which $B_y > 3$nT subtracted days with $B_y < -3$nT for all latitudes at day −5 in the combined MAM and 2-sector structure period. As the behavior of the anomaly does not fit any existing theory, the MC simulations were run 1 million times, just as a test of robustness. As the figure shows, for latitudes 75–80°, the response obtained is outside the probability distribution. This is equivalent to $p < 0.000001$. We conclude that the signal is extremely robust and very unlikely to be produced by chance. To clarify this rather strange anomaly, Figure 13 shows the MAM period for HCSC, where these events are treated to produce differing signed anomalies depending on if it's an "A T" or "T A" event. Since the peak B_y values usually occurs some days after a crossing of the 0-line, the HCSC was considered a potential driver. The crossing events do produce statistically significant positive anomalies in the NH. However, the anomaly still occurs 2 days before the key date, which now represents the day of the HCSC. Another problem with the HCSC is the fact that the 4-sector structures in MAM produce more significance than the 2-sector, while the opposite is true for the correlation between B_y and the pressure. As explained earlier, this could be due to the effect having a non-linear relationship between the strength of the B_y and the surface impact, which could influence how the response in the correlation analysis appears.

Edvartsen et al. (2022) showed how periodic forcing and an autocorrelated response variable will induce an artificial periodicity in the response obtained, even if completely random numbers are used (Fig. 9 in Edvartsen et al., 2022). The results obtained in this study further build on this by showing how two structurally different forcing data series (from 2- and 4- sector structures) exhibit very different degrees of this artificial bias (Fig. 7). This highlights the importance of MC simulation, which is able to take the full autocorrelation function of both forcing and response variables into account. As seen in Figure 8, this leads to the significance distributions being adjusted for the specific periods, and not a one size fits all period. To our knowledge, there exists no method taking this into account as efficiently as MC simulations.

Finally, we will discuss possible hypotheses potentially explaining the lack of significant support of the Mansurov hypothesis and the potential −2 day lag for an HCSC driver.

1. External forcing on the GEC can lead to effects on the internally driven thunderstorm generator. Changes in the GEC could also manifest themselves as changes in the rate of lightning, again leading to atmospheric changes. Changes in the lightning rate at low latitudes can lead to atmospheric disturbances propagating to higher latitudes. Owens et al. (2014) find a statistically significant result for correlations between different IMF polarities and local distribution of lightning. For the toward sector, the lightning rate above the UK is enhanced with respect to the away sector. It is suggested that rather than the annual lightning rate being modulated, a redistribution of the lightning activity with respect to location occurs. However, no definite mechanism is established. Owens et al. (2015) also find results of HCSC correlating at a significant level with thunderstorm activity in the UK over the time period 2000–2007. "A T" crossings are cited to be associated with a strong rise in lightning flash rates immediately following the HCSC. On the contrary, "T A" crossings are cited to be associated with a decrease in flash rates. Both results are statistically confirmed significant by MC-simulation. These results are compelling, as the pressure response also shows asymmetric behavior at the two sector boundary crossings consistent with this study. However, a physical explanation for the −2 day lag in our results is not found. A recommended pathway is a further investigation with improved and prolonged data correlating the IMF B_y and HCSC with the global or local distribution of lightning.

2. The relation is known as the Mansurov Effect is misunderstood. The data does not support the peak B_y as the maximum force, and asymmetry between the hemispheres is also not supported by our analyses. The relation could be non-linear depending on the rate of change of B_y, or both the rate of change of B_y and the maximum B_y in an intricate manner. The pressure response could also have a threshold value before the switching sign as mentioned by Burns et al. (2008). However, for the MAM period (Figs. 5, 11, and 12) the hemispheres have opposite seasons. It can therefore be argued that due to the different atmospheric conditions, this could manifest itself as the same signed responses, even though the forcing itself is asymmetric between the hemispheres.

3. The Mansurov effect exists as it is hypothesized, but the actual effect in the atmosphere is too small to stand out from the noisy background. This is supported by Zhou et al. (2018) showing how the internal thunderstorm generator produces anomalies in accord with the Mansurov effect for the period 1998–2001. However, problems with this specific analysis are the small time period of data and the limited assessment of significance. A better way of detecting the Mansurov effect would be through correlation analyses of the internally generated ionospheric vertical electrical field (E_z) and polar surface pressure. The externally generated changes are suggested to attribute <10% of the total change in Ionosphere-Earth current flow (Tinsley, 2022). If analyses over longer timescales can show the internally generated Ionosphere-Earth current flow (>90% of total) significantly correlating with surface pressure according to the Mansurov hypothesis, one can also assume that external effects will play a role. The external effect might be too small to be detected in a noisy background with the data periods available today, but the existence of statistically significant internal effects would strengthen the hypothesis tremendously.

In addition, as the internal changes are larger, it should also be easier to detect significant changes. These kind of analyses are out of the scope of the article but is a highly recommended pathway for further research on this and related phenomena.

4. The HCSC, not the B_y amplitudes, are responsible for the low altitude pressure correlations. As our results show, HCSC shows up as a statistically significant anomaly in the NH for MAM. However, the significant peak anomaly occurs 2 days before the actual sector boundary crossing. Wilcox et al. (1973) found correlations between the atmospheric vorticity poleward of 20° N and HCSC during the winter months of 1963–1970. These results showed no preference for an "A T" or "T A" crossing and were confined to 500–300 hPa. Figure 13, demonstrates, however, a sector boundary preference. Nevertheless, no mechanism is established for the HCSC correlations termed the Wilcox effect. To our knowledge, there also does not exist recent research on the Wilcox effect. Recommended further research for this pathway would be to look at the correlation between HCSC and pressure for higher atmospheric levels. Before dismissing the physically unjustifiable −2 day lag of the response, it is also recommended to look for solar structures or other phenomena related to HCSC.

5. There exists no physical link between external effects originating from the IMF B_y on the global electric circuit and surface polar pressure. Our analyses show that the sorting of common non-stationary features dependent on the seasons and IMF sector structure gives no statistical evidence in favor of the Mansurov Effect, and the anomaly seen at day −5 could be purely coincidental. However, the extremely low p-values obtained in the NH at MAM are hard to discredit on a statistical basis, especially as the same levels of low p-values are also found for the HCSC. Nevertheless, the responses are also hard to justify on a physical basis with the current knowledge of possible mechanisms rendering a day −2 or −5 lag physically unlikely. An explanation for the discrepancy could therefore also be an aliasing phenomenon. Evidence of the solar rotational UV cycle influencing the Madden–Julian Oscillation (MJO) has been obtained at significant levels after MC simulations (Hood, 2018). The MJO itself is a tropical weather phenomenon, but it has still been shown to impact the Arctic (Zhou & Wang, 2021). Incorporating the MJO oscillation in studies between the IMF and atmospheric pressure is beyond the scope of this paper, but remains a pathway for future research.

5 Conclusion

This study has extended the analyses of the Mansurov effect to possible seasonal and solar wind sector structure-dependent responses on decadal timescales compared to Edvartsen et al. (2022). By correlating the IMF B_y and surface polar pressure, no statistical evidence for dependent behavior is found. However, a new statistically significant anomaly has appeared in multiple sub-periods in both hemispheres. The anomaly occurs approximately 5 days before the maximum B_y value, implying that the effect precedes the forcing, which is not physically justified. We, therefore, provide five different hypotheses as an attempt to explain the phenomena and open pathways for further investigation.

Acknowledgements. We thank the ECMWF (European Center for Medium Weather Forecast) for ERA5 data (https://www.ecmwf.int/en/forecasts/datasets/reanalysis-datasets/era5), NASA Goddard Space Center for OMNIWeb database (https://omniweb.gsfc.nasa.gov/) and Svalgaard (2020) (https://www.leif.org/research/sblist.txt). All codes and data required to reproduce the results of this study are openly available and can be downloaded from Zenodo (https://doi.org/10.5281/zenodo.7851658). The research was funded by the Norwegian Research Council under contracts 223252/F50 (BCSS) and 300724 (EPIC). The editor thanks Maarten Jansen and Jaroslav Urbar for their assistance in evaluating this paper.

References

Benjamini Y, Hochberg Y. 1995. Controlling the false discovery rate: A practical and powerful approach to multiple testing. *J Roy Stat Soc: Ser B (Methodol)* **57**: 289–300. https://doi.org/10.1111/j.2517-6161.1995.tb02031.x.

Burns G, Tinsley B, Frank-Kamenetsky A, Bering E. 2007. Interplanetary magnetic field and atmospheric electric circuit influences on ground level pressure at vostok. *J Geophys Res* **112**. https://doi.org/10.1029/2006JD007246.

Burns GB, Tinsley BA, French WJR, Troshichev OA, Frank-Kamenetsky AV. 2008. Atmospheric circuit influences on ground-level pressure in the Antarctic and Arctic. *J Geophys Res* **113**: D15112. https://doi.org/10.1029/2007JD009618.

Edvartsen J, Maliniemi V, Nesse Tyssøy H, Asikainen T, Hatch S. 2022. The Mansurov effect: Statistical significance and the role of autocorrelation. *J Space Weather Space Clim* **12**: 11. https://doi.org/10.1051/swsc/2022008.

Frederick JE, Tinsley BA, Zhou L. 2019. Relationships between the solar wind magnetic field and ground-level longwave irradiance at high northern latitudes. *J Atmos Sol-Terr Phys* **193**: 105063. https://doi.org/10.1016/j.jastp.2019.105063.

Freeman MP, Lam MM. 2019. Regional, seasonal, and inter-annual variations of Antarctic and sub-Antarctic temperature anomalies related to the Mansurov effect. *Environ Res Commun* **1**: 111007. https://iopscience.iop.org/article/10.1088/2515-7620/ab4a84.

Hood L. 2018. Short-term solar modulation of the Madden-Julian climate oscillation. *J Atmos Sci* **75**: 857–873. https://doi.org/10.1175/JAS-D-17-0265.1.

Kan L, Wu CC. 2021. Characteristics of the heliospheric current sheet at the sector boundaries: Wind observations from 1995–2020. *Astrophys J* **920**: 39 (12 pp). https://doi.org/10.3847/1538-4357/ac1586.

Lam MM, Tinsley BA. 2016. Solar wind-atmospheric electricity cloud microphysics connections to weather and climate. *J Atmos Sol-Terr Phys* **149**: 277–290. https://doi.org/10.1016/j.jastp.2015.10.019. ISSN: 1364-6826.

Lam MM, Chisham G, Freeman MP. 2013. The interplanetary magnetic field influences mid-latitude surface atmospheric pressure. *Environ Res Lett* **8**: 045001. https://doi.org/10.1088/1748-9326/8/4/045001.

Lam MM, Freeman M, Chisham G. 2018. IMF-driven change to the Antarctic tropospheric temperature due to the global atmospheric electric circuit. *J Atmos Sol-Terr Phys* **180**: 148–152. https://doi.org/10.1016/j.jastp.2017.08.027.

Lancaster G, Iatsenko D, Pidde A, Ticcinelli V, Stefanovska A. 2018. Surrogate data for hypothesis testing of physical systems. *Phys Rep* **748**: 1–60. https://doi.org/10.1016/j.physrep.2018.06.001. ISSN 0370-1573.

Mansurov SM, Mansurova LG, Mansurov GS, Mikhnevich VV, Visotsky AM. 1974. North-south asymmetry of geomagnetic and tropospheric events. *J Atmos Terr Phys* **36(11)**: 1957–1962. https://doi.org/10.1016/0021-9169(74)90182-2.

Owens MJ, Scott CJ, Lockwood M, Barnard L, Harrison RG, Nicoll K, Watt C, Bennett AJ. 2014. Modulation of UK lightning by heliospheric magnetic field polarity. *Environ Res Lett* **9**: 115009. https://doi.org/10.1088/1748-9326/9/11/115009.

Owens MJ, Scott CJ, Bennett AJ, Thomas SR, Lockwood M, Harrison RG, Lam MM. 2015. Lightning as a space-weather hazard: UK thunderstorm activity modulated by the passage of the heliospheric current sheet. *Geophys Res Lett* **42**: 9624–9632. https://doi.org/10.1002/2015GL066802.

Russell CT, McPherron RL. 1973. Semiannual variation of geomagnetic activity. *J Geophys Res* **78**: 82–108. https://doi.org/10.1029/JA078i001p00092.

Siingh D, Gopalakrishnan V, Singh R, Kamra A, Singh S, Pant V, Singh A. 2007. The atmospheric global electric circuit: An overview. *Atmos Res* **84(2)**: 91–110. https://doi.org/10.1016/635.

Svalgaard L. 2020. *IMF sector boundaries*. Available at: https://www.leif.org/research/sblist.txt.

Theiler J, Prichard D. 1996. Constrained-realization Monte-Carlo method for hypothesis testing. *Phys D* **94**: 221–235. https://doi.org/10.1016/0167-2789(96)00050-4.

Tinsley BA. 2000. Influence of solar wind on the global electric circuit, and inferred effects on cloud microphysics, temperature, and dynamics in the Troposphere. *Space Sci Rev* **94**: 231–258. https://doi.org/10.1023/A:1026775408875.

Tinsley BA. 2008. The global atmospheric electric circuit and its effect on cloud microphysics. *Rep Progr Phys* **71**: 66801–66831. https://doi.org/10.1088/0034-4885/71/6/066801.

Tinsley BA. 2022. Uncertainties in evaluating global electric circuit interactions with atmospheric clouds and aerosols, and consequences for radiation and dynamics. *J Geophys Res: Atmos* **127**: e2021JD035954. https://doi.org/10.1029/2021JD035954.

Tinsley BA, Deen GW. 1991. Apparent tropospheric response to MeV-GeV particle flux variations: A connection via electrofreezing of supercooled water in high-level clouds? *J Geophys Res* **96 (D12)**: 22283–22296. https://doi.org/10.1029/91JD02473.

Tinsley BA, Heelis RA. 1993. Correlations of atmospheric dynamics with solar activity evidence for a connection via the solar wind, atmospheric electricity, and cloud microphysics. *J Geophys Res: Atmos* **98(D6)**: 10,375–10384. https://doi.org/10.1029/93JD00627.

Tinsley BA, Zhou L, Liu W. 2012. The role of volcanic aerosols and relativistic electrons in modulating winter storm vorticity. *Adv Space Res* **50**: 819–827. https://doi.org/10.1016/j.asr.2011.12.019.

Tinsley BA, Zhou L, Wang L, Zhang L. 2021. Seasonal and solar wind sector duration influences on the correlation of high latitude clouds with ionospheric potential. *J Geophys Res: Atmos* **126(4)**: e2020JD034201. https://doi.org/10.1029/2020JD034201.

Veretenenko S, Ogurtsov M. 2012. Regional and temporal variability of solar activity and galactic cosmic ray effects on the lower atmosphere circulation. *Adv Space Res* **49(4)**: 770–783. https://doi.org/10.1016/j.asr.2011.11.020651.

Veretenenko S, Ogurtsov M, Lindholm M, Jalkanen R. 2018. Galactic cosmic rays and low clouds: Possible reasons for correlation reversal. In: *Cosmic Rays*, IntechOpen, Rijeka, pp. 79–98. https://doi.org/10.5772/intechopen.75428.

Viall NM, DeForest CE, Kepko L. 2021. Mesoscale structure in the solar wind. *Front Astron Space Sci* **8**: 2296-987X. https://doi.org/10.3389/fspas.2021.735034.

Wilcox JM, Scherrer PH, Svalgaard L, Roberts WO, Olson RH. 1973. Solar magnetic structure: Relation to circulation of the Earth's atmosphere. *Science* **180**: 185–186. https://doi.org/10.1126/science.180.4082.185.

Wilks DS. 2016. "The stippling shows statistically significant grid points": How research results are routinely overstated and over interpreted, and what to do about it. *Bull Am Meteorol Soc* **97**: 2263–2273. https://doi.org/10.1175/BAMS-D-15-00267.1.

Williams ER. 2005. Lightning and climate: A review. *Atmos Res* **76 (1–4)**: 272–287. https://doi.org/10.1016/j.atmosres.2004.11.014.

Zhou Y, Wang Y. 2021. Influence of the Madden–Julian oscillation on the Arctic oscillation prediction in S2S operational models. *Front Earth Sci* **9**: 2296–6463. https://doi.org/10.3389/feart.2021.787680.

Zhou L, Tinsley BA, Huang J. 2014. Effects on winter circulation of short and long term solar wind changes. *Adv Space Res* **54**: 2478–2490. https://doi.org/10.1016/j.asr.2013.09.017.

Zhou L, Tinsley BA, Wang L, Burns GB. 2018. The zonal mean and regional tropospheric pressure responses to changes in ionospheric potential. *J Atmos Sol-Terr Phys* **171**: 111–118. https://doi.org/10.1016/j.jastp.2017.07.010.

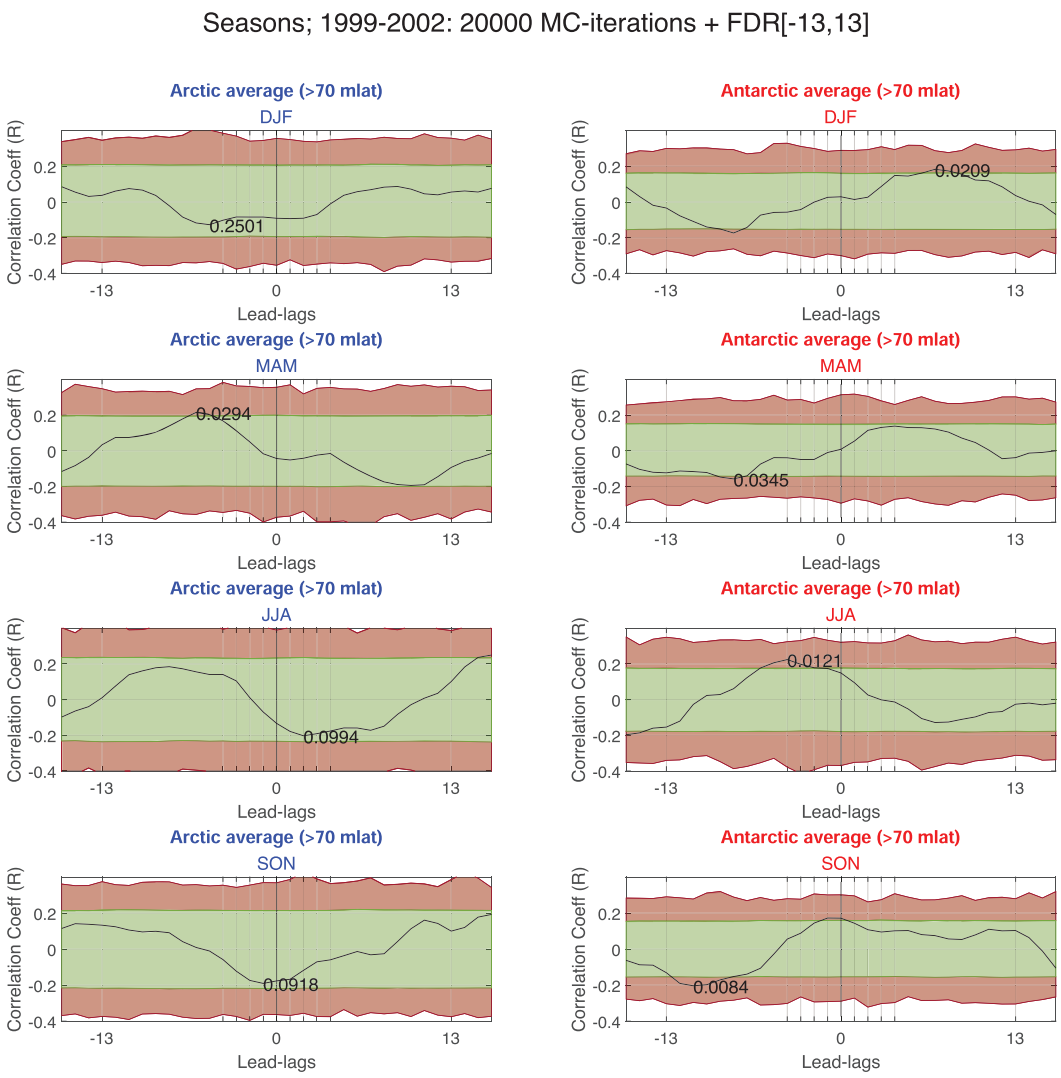

Fig. A.1. *Left panels*: The significance level for the time-lagged cross-correlation after 10,000 MC-iterations for the period 1999–2002 in the NH for the months DJF (top panel), MAM (middle top panel), JJA (middle bottom panel) and SON (bottom panel). FDR interval is set between lead and lag −13 to +13. *Right panels*: Same procedure, only for the SH. No significance is observed after the FDR method.

Appendix

A similar analysis as done in Section 3.2 (seasonality) is performed for the most cited period of 1999–2002 and shown in Figure A.1. It is noted that due to the small time period (implying cheaper computations for the MC simulation), we perform 20,000 MC iterations for increased accuracy. Tinsley (2022) discuss how the mixing of the seasons might affect the significance assessment, due to favorable conditions for the Mansurov effect in the local wintertime. However, as the figure shows, no specific season has a statistically significant response when the FDR is applied over the interval −13 to +13 lead-lags.

A similar analysis as done in Section 3.5 (sector structure) is performed for the most cited period of 1999–2002 and shown in Figure A.2. No specific sector structure shows a statistically significant response when the FDR is applied over the interval −13 to +13 lead-lags.

A similar analysis as done in Section 3.6 (seasons and sector structure) is also performed for the most cited period of 1999–2002 and shown in Figure A.3. No specific combination of season and sector structure shows a statistically significant response when the FDR is applied over the interval −13 to +13 lead-lags. The most notable anomaly occurs in the Arctic for the JJA period in 4- or irregular sector structures. Here, the negative anomaly on day 1 obtains a p-value equal to 0.0061. It is noted that if the FDR method is only performed over the interval −2 to +2 lead-lags the anomaly at day 1 would be rendered statistically significant. However, this result is not in line with the hypothesized mechanism being favored in local winter and 2-sector structures (Tinsley, 2022), as the result would be significant in the opposite combination (local summer and 4- or irregular sector structures). A reasonable explanation for this result might very well be appointed to chance. For the FDR interval set to −2 to +2 lead-lags, this particular response

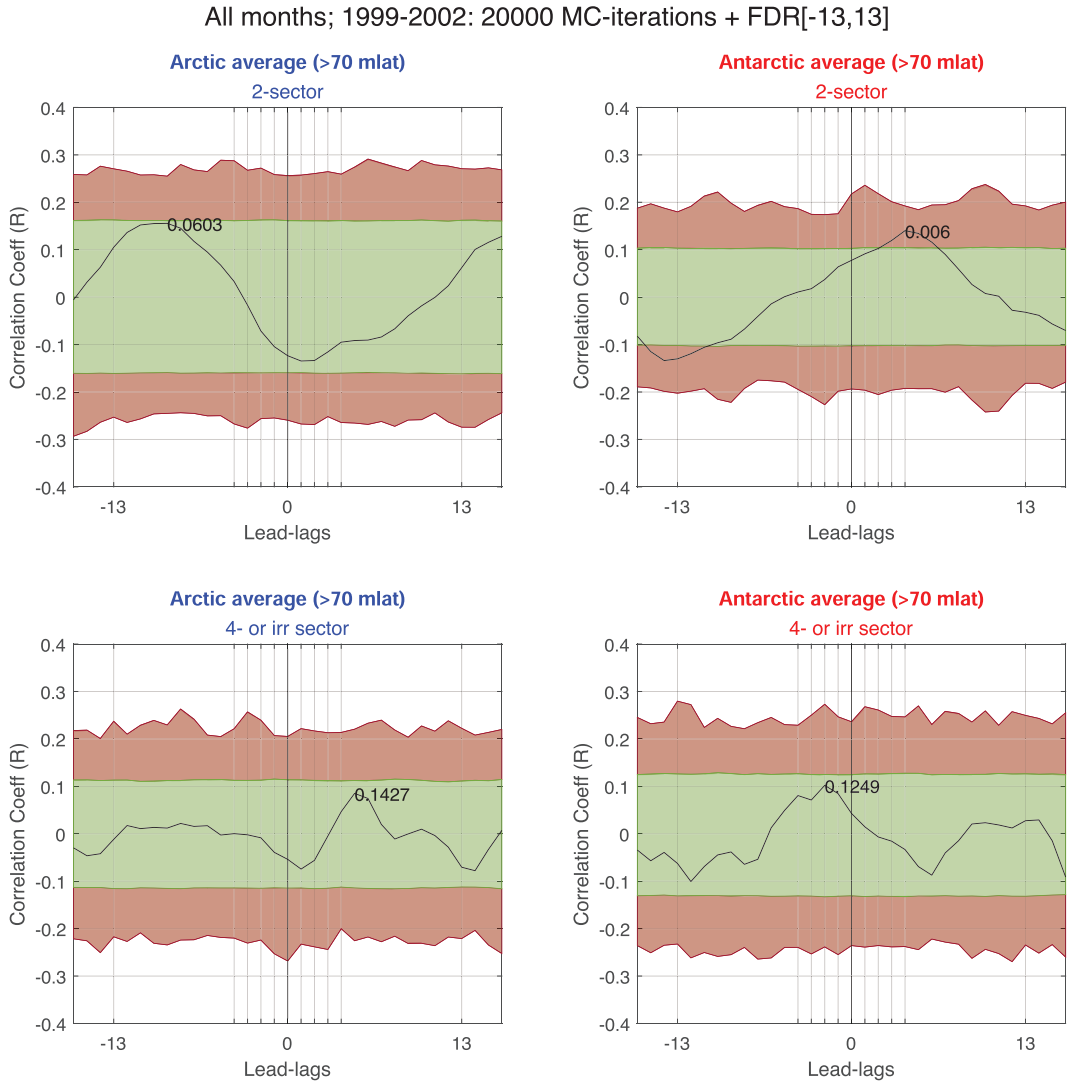

Fig. A.2. *Left panels*: The significance level for the time-lagged cross-correlation after 10,000 MC-iterations for the period 1999–2002 in the NH for 2-sector structures (top panel)/4- or irregular sector structures (bottom panel). FDR interval is set between lead and lag −13 to +13. *Right panels*: Same procedure, only for the SH. No significance is obtained in either hemisphere.

is per definition statistically significant as only 5% of rendered responses will have equally low *p*-values within this interval. However, as the figure display a total of 16 subplots, this means that the expected value of getting 1 signal that passes the FDR limit is 16/20 = 0.8. Based on the premise that this particular period does not fit the hypothesized mechanism, it is therefore reasonable to assume that this might occur by chance. Nevertheless, as discussed in Section 3.8 (Heliospheric Current Sheet Crossings), the most significant responses are seen under the 4-sector structures. A mechanism including crossing events might then give an explanation for this occurence.

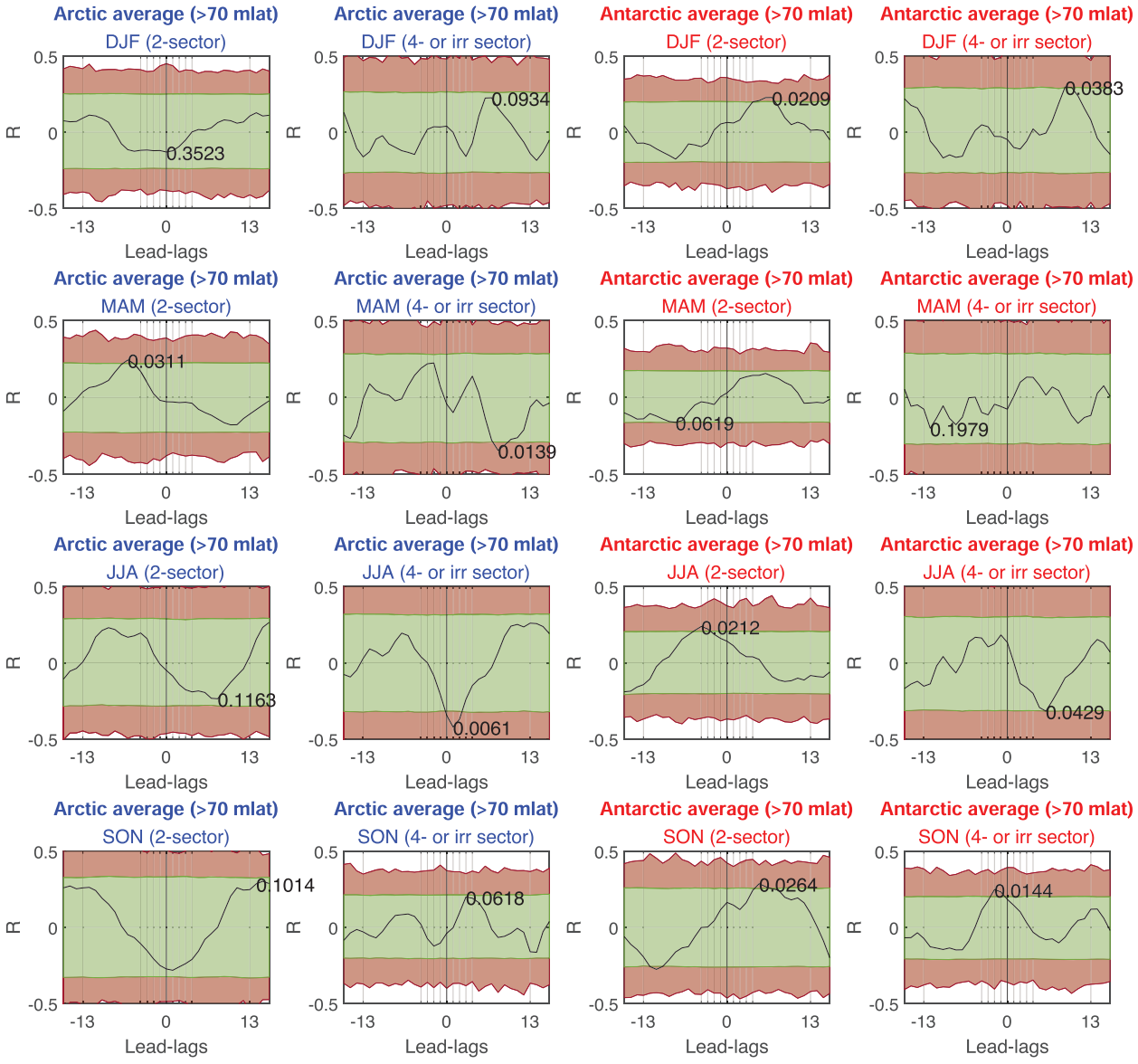

Fig. A.3. *Left panels*: The significance level for the time-lagged cross-correlation after 10,000 MC-iterations for 2-sector structures in the period 1968–2020 in the NH for the months DJF (top panel), MAM (middle top panel), JJA (middle bottom panel), and SON (bottom panel). FDR interval is set between lead and lag −13 to +13. *Left middle panels*: Same procedure for the 4-or irregular sector structures in the NH. *Right middle panels*: Same procedure for the 2-sector structures in the SH. *Right middle panels*: Same procedure for the 4-or irregular sector structures in the SH. No significance is observed in either hemisphere.

Cite this article as: Edvartsen JØ, Maliniemi V, Nesse H & Hatch S 2023. The Mansurov effect: Seasonal and solar wind sector structure dependence. *J. Space Weather Space Clim.* **13**, 17. https://doi.org/10.1051/swsc/2023013.